ROYAL SOCIETY
OF CHEMISTRY

REVIEW

Check for updates

Hard carbon for sodium-ion batteries: progress, strategies and future perspective

Chun Wu, [ID] [ab] Yunrui Yang, [ac] Yinghao Zhang, [ac] Hui Xu, [b] Xiangxi He, [a] Xingqiao Wu [ID] *[ac] and Shulei Chou [ID] *[ac]

Because of its abundant resources, low cost and high reversible specific capacity, hard carbon (HC) is considered as the most likely commercial anode material for sodium-ion batteries (SIBs). Therefore, reasonable design and effective strategies to regulate the structure of HCs play a crucial role in promoting the development of SIBs. Herein, the progress in the preparation approaches for HC anode materials is systematically overviewed, with a special focus on the comparison between traditional fabrication methods and advanced strategies emerged in recent years in terms of their influence on performance, including preparation efficiency, initial coulombic efficiency (ICE), specific capacity and rate capability. Furthermore, the advanced strategies are categorized into two groups: those exhibiting potential for large-scale production to replace traditional methods and those presenting guidelines for achieving high-performance HC anodes from top-level design. Finally, challenges and future development prospects to achieve high-performance HC anodes are also proposed. We believe that this review will provide beneficial guidance to actualize the truly rational design of advanced HC anodes, facilitating the industrialization of SIBs and assisting in formulating design rules for developing high-end advanced electrode materials for energy storage devices.

1. Introduction

At present, the energy and environmental issues caused by burning fossil fuels have prompted researchers to search for much cleaner energy sources. However, the development of energy storage equipment is of great significance to overcome the characteristics of discontinuity and instability of clean energy, including wind and solar energy.[1–3] Among the various energy storage devices, SIBs with unique features, such as abundant resources and high cost performance, have been regarded as the most competitive candidates.[4–7] Compared with traditional lithium-ion batteries (LIBs), SIBs exhibit great advantages in terms of resources and cost, resulting in distinct application scenarios (Fig. 1a and b).[8–10] However, the properties, cost, performance and reliability of SIBs largely rely on their electrode materials, and thus, the preparation of high-performance electrode materials holds immense scientific and practical significance (Fig. 1c).[11,12]

In this case, anode materials as one of the key components of SIBs can be typically categorized into four main types,

i.e. carbon-based materials,[13–15] metal oxides,[16,17] alloys and organic matters (Fig. 2a).[18,19] However, a large number of the above-mentioned materials have the shortcomings of complex preparation processes and unsatisfactory electrochemical features and, therefore, are not suitable for practical application, thus deviating from the original goal of SIBs. Due to their abundant resources, low cost and simple production, carbon-based materials are recognized as the most desirable candidates for SIBs, including soft carbon (SC) and HC.[20,21] However, SC is less competitive because of its high degree of graphitization and corresponding limited interlayer spacing distance, leading to a relatively low ICE.[22,23] In contrast, HCs with a large scope for the regulation of their microstructure and high reversible specific capacity are regarded as the most likely commercial anode materials for SIBs and have thus received significant attention in recent years (Fig. 2b and c). However, some critical issues still need to be addressed, for example, their undesirable ICE, electrochemical performances and cost.[24,25] It is worth noting that their preparation process has a significant impact on their cost. As described in the routine preparation step, raw material treatment (crushing, purification and drying), pre-carbonization, secondary carbonization and high energy consumption are needed in a typical high-temperature carbonization process.[26] Consequently, ensuring electrochemical performance, reducing energy consumption and simplifying the process seems to be a big challenge. Although numerous high-performance HC

[a]Wenzhou Key Laboratory of Sodium-Ion Batteries, Wenzhou University Technology Innovation Institute for Carbon Neutralization, Wenzhou, Zhejiang 325035, China

[b]College of Materials Science and Engineering, Changsha University of Science and Technology, Changsha 410114, China

[c]Institute for Carbon Neutralization, College of Chemistry and Materials Engineering, Wenzhou University, Wenzhou, Zhejiang 325035, China. E-mail: xingqiaowu@wzu.edu.cn; chou@wzu.edu.cn
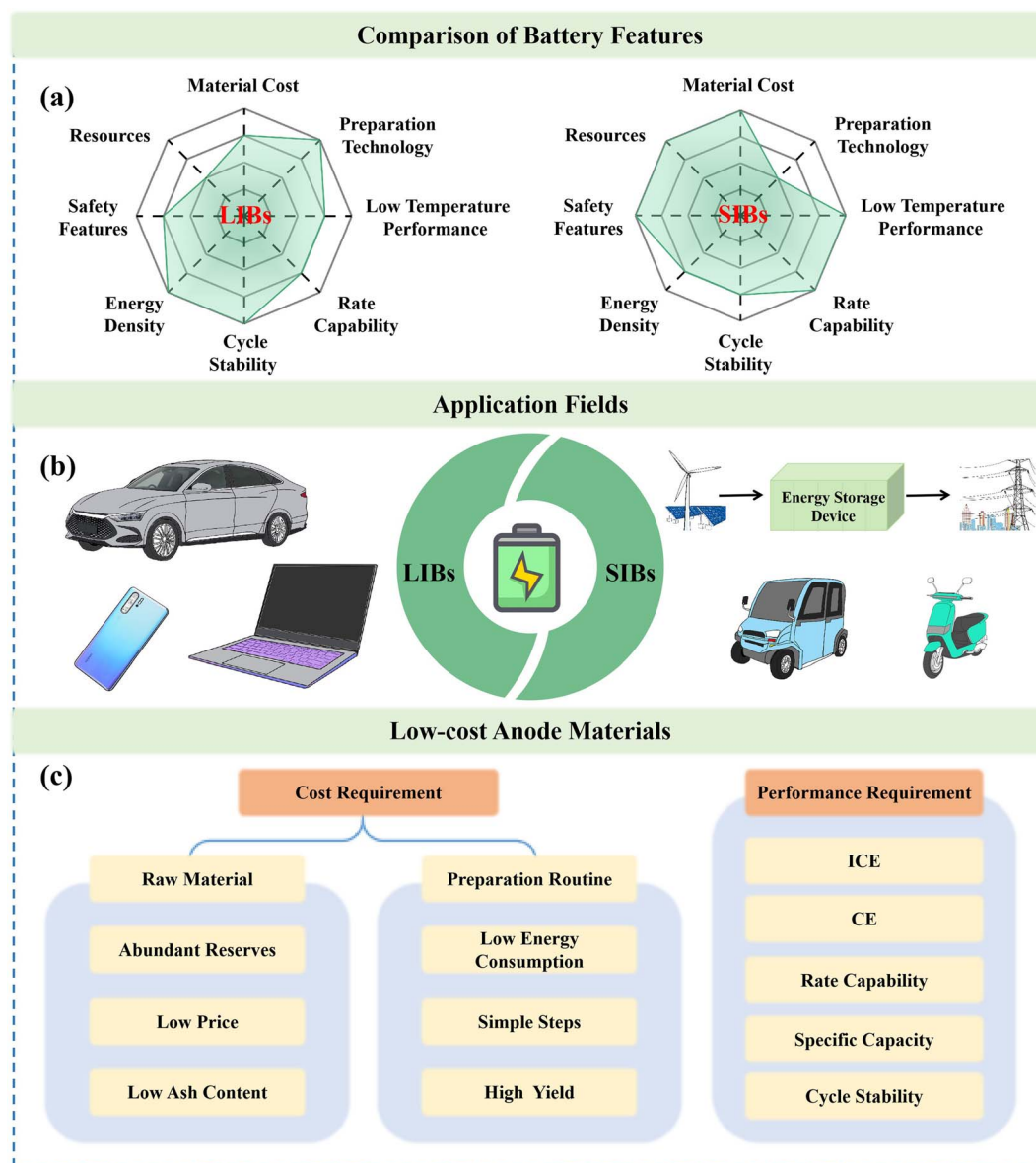
Fig. 1 (a) Comparison of battery features, (b) application fields and (c) low-cost anode material requirements for LIBs and SIBs.

anodes have been reported at the laboratory level, it is still unknown whether they are useful for the commercialization of HCs.

In this regards, herein, recent advancements in the preparation approaches for HC anode materials are concisely overviewed and some typical representative works are summarized. Firstly, the development and classification of traditional fabrication methods for HC anodes and their corresponding Na storage behaviors are briefly introduced. Next, advanced strategies, including high-temperature carbonization methods, pretreating and post-treating methods, are highlighted. Besides, the physical and electrochemical performance of HC anodes and their full cells are also discussed in detail. Meanwhile, a comparison between traditional fabrication methods and advanced strategies is systematically presented (Fig. 3). Finally,

challenges and future development prospects to achieve high-performance HC anodes are further proposed. To date, most research is focused on traditional methods for the preparation for HCs, including regulating the temperature and heating rate, which can be named as the "inherent comfort zone". Here, this review is aimed at proposing new preparation strategies and conducting a deep exploration based on this, and stepping out of the original "comfort zone". Only with more researchers invested in this type of investigation that the improvement and development of new preparation strategies can be promoted. By aggregating the most cutting-edge and promising methods, the industry of SIBs will be pushed forward. By summarizing the most cutting-edge and promising methods, the target of boosting the progress of the industrialization of SIBs can be realized.
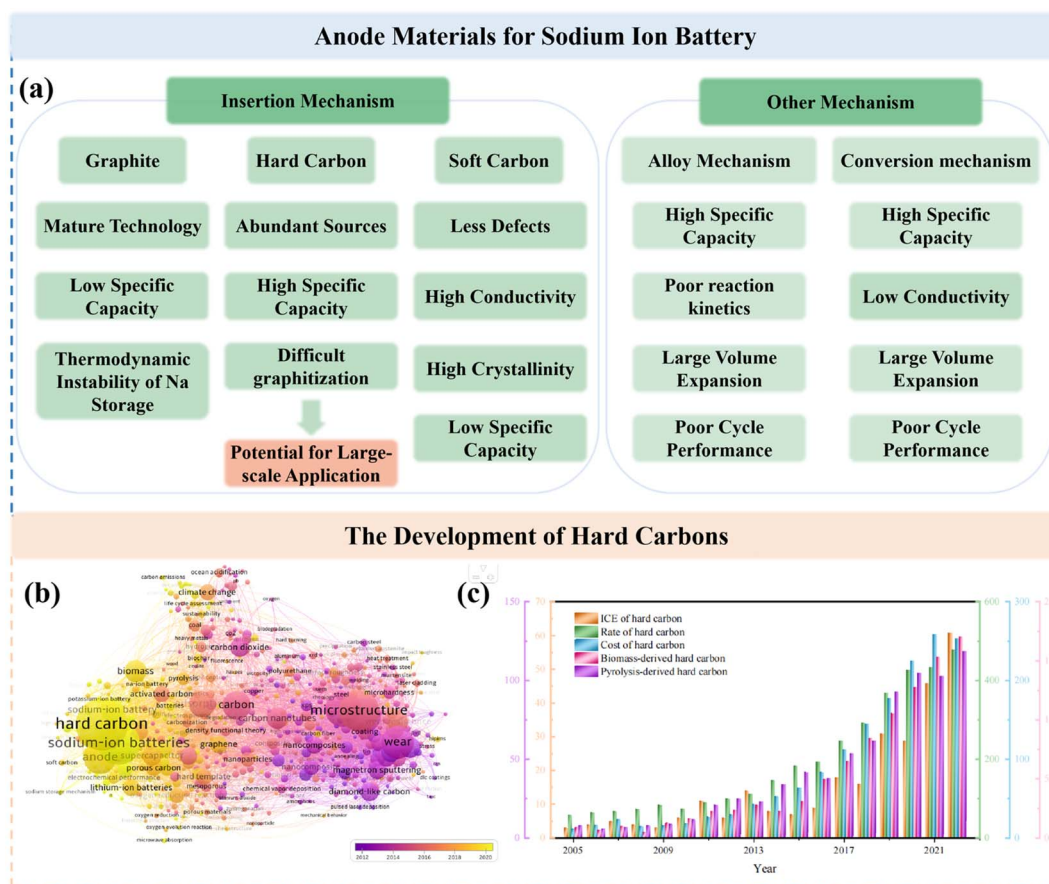
Fig. 2 (a) Comparison of anode materials for SIBs, (b) hotspot of hard carbon anode materials for SIBs from 2010 to July 2023, and (c) the development of keywords for hard carbons (the data were collected *via* Web of Science, July 2023).
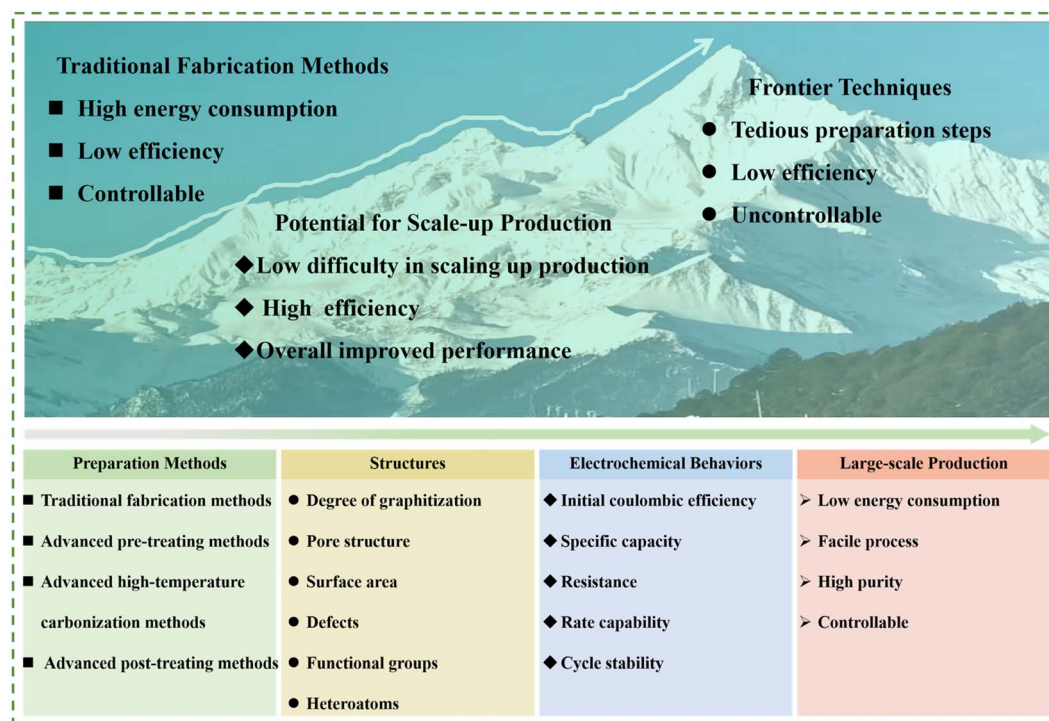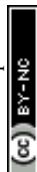

Fig. 3 Comparison between traditional fabrication methods and advanced strategies.

2. The development process with sodium storage mechanism and performance

Actually, HC anodes employed in SIBs display similar electrochemical behavior to the graphite anode in LIBs, which exhibit long and reversible charge/discharge plateaus under 0.1 V. The first work on HC anodes for SIBs can be traced back to 2000, where Stevens and coworkers prepared glucose-derived HCs, showing a reversible capacity of about 300 mA h g^{-1}, and the significantly important "house of cards" model for sodium/lithium storage in HCs was proposed.[27] Since then, researchers have devoted extensive efforts to creating various HCs from different precursors and with distinct preparations conditions, and consequently exceptional achievements have been delivered.[28–30] It has been documented that the microstructure of HCs is complicated, which consists of a large number of disordered microcrystalline carbon layers stacked randomly. Specifically, one part of the carbon layers is arranged in parallel to create graphitic microcrystalline regions and the other part of the carbon layers is arranged in a disordered manner to form nano-sized microporous regions.[31] Furthermore, the surface structure of HCs is also complex, which including the type of carbon atom bonding, the ratio of edge plane to basal plane, chemically or physically adsorbed functional groups, doped atoms and defects.[32] Consequently, different Na$^+$ storage mechanisms are derived from these characteristics of HCs. With more advanced technical methods, the sodium storage mechanisms have been investigated in detail. In general, these sodium storage mechanisms are basically divided into adsorption, intercalation, pore filling, and sodium cluster formation process, and the development of these mechanisms are presented in Fig. 4a.[27,33–39] At present, high-capacity HC is based on the control of the platform region below 0.1 V or 0.05 V. It is worth noting that the preparation process has a significant impact on the microstructure of HCs, including their degree of graphitization, pore structure, surface area, defects, and functional groups, which often directly determines the upper limit of the final Na storage performance (Fig. 4b).

3. Traditional fabrication methods

HCs are regarded as the most promising anode materials for SIBs and have received tremendous attention in recent years. They represent carbon materials that cannot be transformed into graphite at high temperature with complicated microstructures and surfaces (Fig. 5a), which are commonly derived from sugars, biomass, or polymers and typically prepared via one-step direct heating, microwave irradiation or hydrothermal carbonization, followed by further pyrolysis treatment at 1000–2000 °C in a tubular furnace for several hours.[40] Consequently, the pyrolysis procedure has an essential impact in tuning the microstructure of HC anode materials, such as their interlayer distance, number of stacking layers, number of defects, pore structures, specific and surface area, and furthermore will undoubtedly further affect their Na storage properties

(Fig. 5b).[41] It can be obviously seen in Fig. 5c that the specific capacities reached the maximum value at around 1200–1600 °C, which can be ascribed to the balanced proportions of the defect-derived adsorption capacity and the graphitic domain-derived intercalation capacity. Besides, the ICE for most HC anodes is no higher than about 80% (Fig. 5d). With an increase in the pyrolysis temperature, the ICE increases as a result of the decreased amount of defects, and thus lowers the irreversible capacity.[42–86] In summary, high-temperature pyrolysis treatment is a necessary step to ensure the graphitization structure of the final products. However, different pre-treatments are applied to achieve desirable performance according to different precursors. Thus, various types of treatments will lead to different electrochemical behaviors, but they exhibit consistent changing trends (Fig. 5c and d). Therefore, the regulation of the carbonization process, and even the synthesis approaches are critical for improving the properties of HC.

3.1 One-step method

Direct carbonization at the target temperature with a low heating rate and long duration is regarded as the most common strategy to produce HC anode materials. The first work on the preparation of HC under direct carbonization treatment was reported by Dahn et al., which was a typical process by heating dehydrated glucose to 1000 °C in Ar.[27] Their investigation revealed that Na can be inserted into the interlayer space in disordered carbon materials according to in situ wide-angle X-ray scattering measurement, which was confirmed through the increase in the interlayer spacing in these HC materials. In addition, in situ small-angle X-ray scattering (SAXS) characterization obviously presented the insertion process of Na in the nanopores within disordered HCs. A reversible capacity about 300 mA h g^{-1} was delivered, which was much higher than that of the graphite anode in SIBs. This work pioneered the research on HC anode materials in SIBs and laid the foundation for the further study of non-graphite anode materials.

Afterwards, considerable research has been reported utilizing the same method to obtain HC anode materials.[35,47,87] A superior low-cost pitch and lignin-derived HC anode was prepared in the temperature range of 1200–1600 °C by Hu and coworkers.[47] The optimized HC with suitable microstructure and morphology exhibited exceptional electrochemical behaviors in terms of satisfied ICE (82%), high reversible capacity (254 mA h g^{-1}), and outstanding cycle stability. After that, they reported the preparation of an HC material with a microtubular shape prepared from natural cotton by carbonization at 1300 °C, achieving a low specific surface area of 38 m^2 g^{-1}.[35] Physical measurements, such as SEM, TEM, Raman, XRD, and N$_2$ adsorption, were applied to elucidate the correlation between the electrochemical performance and structure. Based on the hollow fibrous structure, the ionic diffusion distance effectively decreased in the resulting HC anode, and consequently a high reversible capacity about 315 mA h g^{-1} and desirable ICE of 83% were delivered in SIBs. After that, another novel popular wood-derived HC with improved reversible capacity of 330 mA h g^{-1} and enhanced ICE of 88.3% was discovered by the same group.[88]
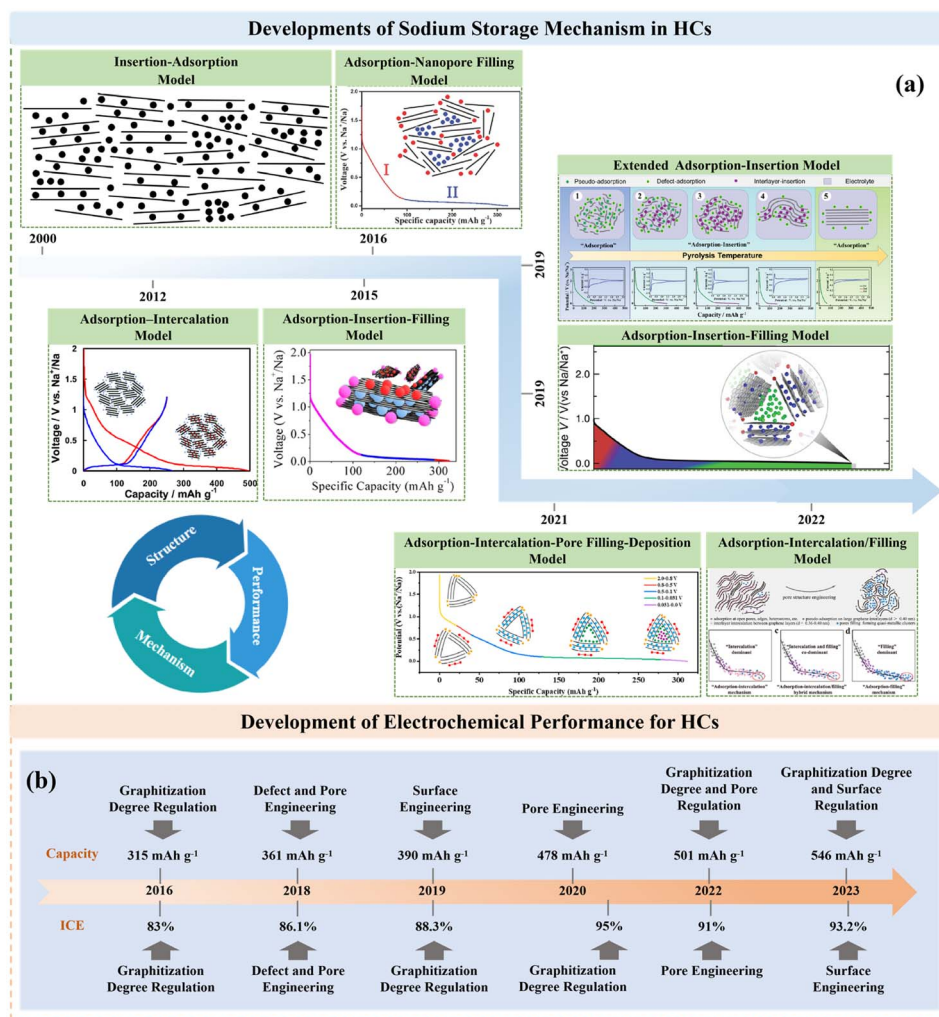
Fig. 4 Timeline of key developments in the sodium storage mechanism (a) and electrochemical performance (b) of HCs.

Another meaningful work on HCs originating from a sucrose precursor prepared in the temperature range of 700 °C to 2000 °C, which were applied in LIBs, SIBs and PIBs, was reported by Komaba and coworkers. XRD, Raman, SAXS, electron spin resonance spectroscopy, electron microscopy, and pair distribution function analysis were employed to systematically observed the particle morphology and structures of the HC materials.[69] The characterization showed that increasing the heating temperature led to a reduction in the amount of defects and increase in the amount of ordered structures inside the HC materials (see Raman spectra). Some structural parameters of the HC anode obtained under different temperatures were presented and the illustration of its evolution with an increase in temperature exhibited. When evaluated as an anode for LIBs, SIBs and potassium-ion batteries (PIBs) in non-aqueous systems, the electrochemical properties of the HCs demonstrated significant differences depending on their synthesis temperatures and alkali-metal ions. Based on the observations, approaches to achieve advanced HC anodes for high energy density LIBs, SIBs and PIBs were also discussed.

3.2 Two-step method

The precursors, including biomass, pitch-based materials and polymers, are the current relatively mature choice for the commercialization of HCs. The production process of biomass-based HCs is relatively simple, but how to screen suitable precursors and realize stable bulk supply are the main challenges. In contrast, HCs derived from pitch-based precursors are currently more difficult to produce and exhibit a poorer performance than biomass-based HCs, but their supply of raw materials is relatively stable. With the breakthrough of research and development technology for precursors and the application of other material modification technologies, these HCs with wide supply sources and low cost will achieve large-scale applications. Additionally, with phenolic resin, it is easier to regulate the crosslinking degree from the original material and a high reversible capacity can be achieved, but the cost of pyrolysis and crosslinking of the raw material to get the pre-carbonization material is high. Specifically, coconut shell-derived HCs, which are regarded as the fastest industrialized product currently, present an ideal electrochemical
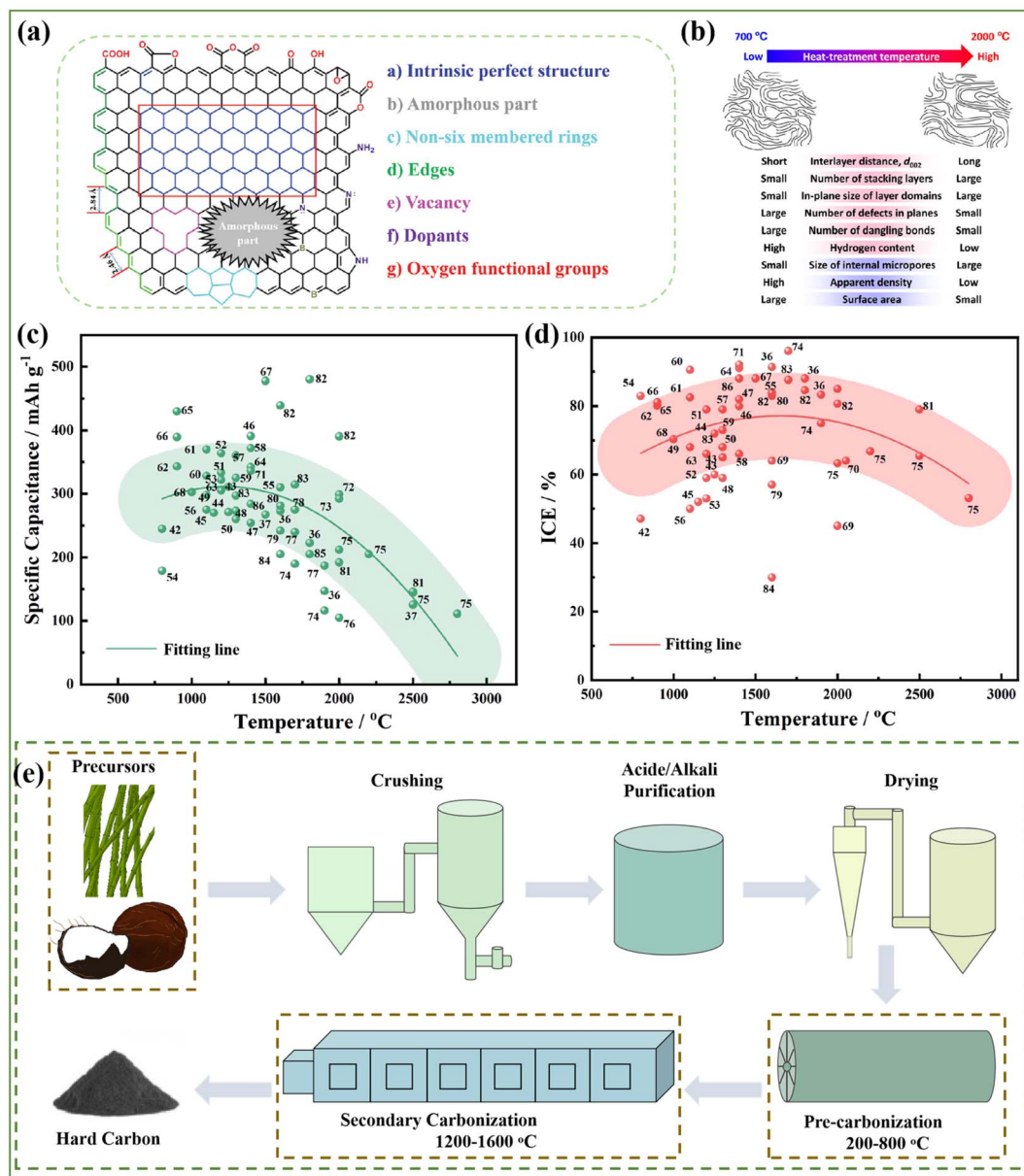
Fig. 5 (a) Illustration of carbon surface with different types of defects. (b) Diagram of structural parameters for HC synthesized at 700 °C and 2000 °C. (c and d) Relationship of specific capacity and ICE with the pyrolysis temperature of HCs based on published works. (e) Schematic illustration of the main steps for a mature route to HC commercialization.

performance, but it is difficult to guarantee their demand for application in SIBs for a long time. Generally, the route for the large-scale production of HCs includes the following main steps (as presented in Fig. 5e): selection of precursor (bamboo, starch, coconut shell, *etc.*), pulverization (different particle sizes), purification (different solvents), drying (various drying methods), pre-carbonization (different heating rates and target temperatures) and secondary carbonization treatment (different heating rates and target temperatures).[26] It has been proven that impurities in the precursors of HCs is the main reason resulting in the degradation of their specific capacity and other electrochemical behaviors. Accordingly, effective strategies to eliminate these impurities are urgently needed. In general, utilizing water and acid and alkali solution for washing

before high-temperature treatment is regarded as a common way to acquire desirable HC materials.[89–93] For example, Adamson and coworkers proposed a method of treatment with KOH and HCl solutions after pre-pyrolysis, and finally post-pyrolysis for the preparation of peat biomass-derived HCs.[94] Given the advantages of the two aforementioned solutions, the improvement in the electrochemical performance for peat-derived HCs was remarkable in terms of specific capacity and ICE. Another extraordinary achievement about the enhancement of ICE (91%) with fabulous reversible specific capacity (342 mA h g^{-1}) was reported by our group employing hazelnut shell as the precursor.[64] It has to be clarified that the organic composition could be obviously modified and the inorganic ingredient favourably removed in the hazelnut shell precursor,
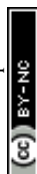
and under the combination of these two aspects, the amount of micropores was effectually reduced and a low specific surface area was achieved. The N_2 adsorption–desorption isotherms analysis revealed that HCl-1400 possessed a lower specific surface area and less micropores compared with that of the 0M-1400 sample, which was responsible for preventing the decomposition of the electrolyte and subsequent generation of an SEI layer. XPS and XRD measurements showed that with HCl treatment, the chemical component and microstructure in the resultant HCs, such as active sites and interlayer spacing, changed, which were beneficial for improving the Na storage performance.

Among the aforementioned commercial preparation steps, pre-carbonization and secondary carbonization treatment employ two different furnaces separately, which is conducive for the long lifespan of the secondary carbonization furnace. Actually, introducing pre-carbonization treatment before direct carbonization has been proven to be an important method to tune the configuration of oxygen functional groups, which can play an important role in the performance of HCs applied in SIBs. More importantly, the amount of volatiles can be reduced by pre-treatment. Typically, closed micropores and carbonyl groups were successfully generated simultaneously in bamboo-derived HCs through a pre-carbonization process at 500 °C for 2 h, and subsequently at 1300 °C for 2 h in Ar, as apparently observed from the N_2 adsorption and XPS results.[86] It was stated that the closed micropores favored Na storage in the plateau region, while the carbonyl groups were conducive to boosting the reversible Na adsorption capacity in the slope region. Under the combination of the two aforementioned aspects, the optimized specific capacity about 348.5 mA h g^{-1} at 30 mA g^{-1} with an ICE about 84.1%, and advanced cycle stability about 91.6% capacity retention at 300 mA g^{-1} over 500 cycles were delivered. This novel investigation offers guidance for accurately designing the microstructure of biomass-derived HCs. Actually, the typical example for pre-carbonization and subsequent high-temperature carbonization process to regulate the pore structure dates back to the research by Hu and coworkers in 2019.[95] A hierarchical porous waste cork-derived HC anode was successfully prepared owing to the natural holey texture inside the precursor. Specifically, the detailed analysis based on SAXS with effective skeletal density test revealed that the number of open pores was reduced and the number of closed pores increased with an increase in the pyrolysis temperature, which corresponds to the initial capacity loss and plateau capacity, respectively. These special structure features endowed the half-cells with desirable Na storage behavior, exhibiting a specific capacity of about 360 mA h g^{-1} and practical application ability in full-cells with a high energy density of about 230 W h kg^{-1} with 71% capacity retention over 2000 cycles.

3.3 Other methods

In the case of the biomass precursors, direct carbonization treatment seems to be a straightforward way to prepare HC anode materials. However, some unique microstructures of HCs derived from sugars or polymers, such as spheres and nanowires, with a desirable packing density, good structural stability and low surface to volume ratio have demonstrated great potential to be optimal candidate anodes for SIBs.[96,97] Generally, the common approaches to prepare these special structures of HCs are based on a two-step process, hydrothermal carbonization or microwave irradiation treatment, and subsequent high-temperature carbonization procedure.

According to Lust et al., HC spheres with a narrow size distribution were synthesized through hydrothermal carbonization and subsequent pyrolysis at 1100 °C by applying the precursor of D-glucose.[96] Specifically, the SEM images showed that the as-prepared HCs possessed a relatively smooth surface and micrometer-size interconnected spherical structure, which was the unique feature of the materials prepared via the hydrothermal carbonization process. When evaluated in 1 M $NaClO_4$ propylene carbonate electrolyte system, a capacity of about 300 mA h g^{-1} was achieved in the first cycle and about 160 mA h g^{-1} maintained after 200 cycles. Meanwhile, it could be obviously noted the HCs exhibited high reduction and oxidation peaks of Na in their cyclic voltammograms. The accumulation of Na on/in the electrochemically polarized porous nanosphere HCs was clarified from the physical measurements. Furthermore, the charge transfer resistance, mass transfer characteristics and total polarization at the electrode/electrolyte interface were noticeably influenced.

In another example, HC microspheres were prepared by Liu and coworkers through a similar process but using various heating rates of 5, 2, 1, or 0.5 °C min^{-1}.[98] As a result, it was demonstrated that a low heating rate had a significant effect on the concentration of defects in the as-obtained HCs. In particular, the N_2 adsorption–desorption behaviors and Raman spectroscopy indicated that the HC-0.5 electrode showed non-detectable porosity and the lowest defect concentration. Further, electrochemical measurements illustrated the exceptional Na storage properties in terms of satisfactory ICE (86.1%), ultrahigh specific capacity (361 mA h g^{-1}) and desirable cycle stability (94% after 100 cycles). Additionally, it was also predicted from theoretical simulation that the continuous Na ion flux can be disrupted by the existence of defects via trapping Na ions and creating a repulsive electric field. These fundamental studies can not only offer an explanation for the influence of defects on the Na storage performance, but also shed light on the significant regulation principles of high-performance HCs for SIBs.

More recently, a systematically investigation on the critical influence of the hydrothermal carbonization process on regulating the microstructure of HCs for SIBs was firstly elucidated by Titirici and workers.[97] It was concluded that the hydrothermal process favored high carbon yields, reduced carbon emissions and conferred more active sites including defects and closed nanovoids inside HCs, which are favorable for an improved electrochemical performance. The as-obtained HCs synthesized under the optimal conditions showed an ultrahigh discharge capacity of about 420 mA h g^{-1}. When constructed with an $Na_3V_2(PO_4)_3$ (NVP) cathode, the fantastic reversible capacity of about 318.2 mA h g^{-1} can be achieved 3.5 V for the full-cell. Furthermore, a superior high energy density of 237.8 W h kg^{-1} could be delivered. Overall, the hydrothermal

process has been proven to be a useful pre-treat step with real sustainability feature, promoting the electrochemical behavior of SIBs. However, this typical method is not suitable for large-scale production because of the high pressure involved.

Typically, compare to the hydrothermal carbonization treatment, another more effective way is microwave irradiation synthesis, which can uniformly heat the reactant to a high temperature in a short time by transferring energy selectively to the microwave-absorbing polar solvents. Therefore, it is an energy and time-saving method.[99–101] In this regard, Chen and coworkers developed carbon microspheres (CSs) from a sucrose precursor through the microwave-assisted approach.[102] It was suggested that their unique spherical structure was beneficial for mass transport and storage, and consequently the as-prepared CSs displayed a high specific capacity, excellent cycle life and good rate capability. Similarly, Puravankara et al. synthesized HC microspheres (HCMS) from a sucrose precursor and a 50% DEG/H$_2$O solvent mixture using the microwave technique and subsequent high-temperature carbonization process.[103] The insertion/pore-filling mechanism under 0.1 V was validated and the defect/vacancy-assisted adsorption/insertion and insertion/micropore filling Na-ion storage mechanism in HCs was also asserted by different HCMS samples. It was verified that organic xerogels (OXs) can complete the gelation and ageing process when the carbon precursor placed in a microwave oven.[104] Adopting this method, carbon xerogels (CXs) with an analogous chemical composition and BET surface area but different textural features (10–200 nm) were prepared by Cuesta et al.[104] and the influence of their textural characteristics on the performance of SIBs investigated, which revealed the feasible application of these unique CXs to achieve promising HC anodes for SIBs. Previous studies revealed that the microwave-assisted method is an effective, rapid and low-energy consumption procedure to achieve HCs, but it still remains a significant issue to solve how to precisely control the heating effects due to the fact that the rapidly alternating electromagnetic field is difficult to regulate, and the interactions between microwaves and conductive materials are also complex.

Overall, notable progress has been made in the development of HCs via traditional methods, but it also should be noted that there are still many existing issues, for example, the range that can be regulated is limited, where it has been documented that basically only the heating rate during the temperature and the target secondary carbonization temperature can be tuned. Hence, it is urgent to develop new approaches to achieve high-performance HCs for SIBs.

4. Advanced strategies

Recently, numerous novel and advanced methods for the preparation of HCs have been reported, which exhibit scalable, efficient, and rapid characteristics as well as excellent electrochemical performance of the resultant HC anodes in contrast to that of the traditional strategies. Specifically, recent research on advanced pre-treatment methods, advanced high-temperature carbonization methods and advanced post-treating methods will be introduced in this section.

4.1 Advanced pre-treatment methods

It has been documented that the pre-treatment process of the HC precursor is proven to be a meaningful way towards promoting the Na storage property of HCs. In the current mass production process, pre-carbonization treatment is usually adopted to achieve the requirement of a reduction in volatility, but it shows limited effects for structural modulation. Therefore, other pre-treatments are urgently needed. In general, the reported works with significantly improved performances employed some typical approaches including low-temperature hydrogen reduction and pre-oxidation.[59,61,105]

4.1.1 Low-temperature hydrogen reduction.
Besides carbon, oxygen is the most common element presented in various precursors, which gradually escapes at high-temperature treatment and exerts a great impact on the final microstructures of the as-prepared HCs, further affecting the electrochemical behaviors of SIBs. Nevertheless, little attention has been paid to this issue according to previous reports. Based on this, Chen and workers chose esterified starch as the precursor and precisely tuned its oxygen content via a low-temperature hydrogen reduction process (as seen in Fig. 6a).[61] The physical measurement analysis, as shown in Fig. 6b–d, revealed that it can boost the closure of open pores and realize the orientated alignment of carbon layers at 1100 °C with a decrease in the content of oxygen of precursors but guarantees the stability of crosslinking structures, as proven via N$_2$ adsorption, XRD, Raman and XPS. The results showed that a high proportion of pseudo-graphitic domains and low specific surface area of 2.96 m^2 g^{-1} were achieved for the optimal HC anode material, which contributed to the desirable electrochemical performance and related mechanism interpretation for the Na storage behaviors. Moreover, a high energy density (243.1 W h kg^{-1}) for a full cell (Fig. 6e–g) was acquired when assembled with a NVP cathode, elucidating its great practical potential for SIBs. The same method was also applied by Ru and coworkers employing 3D hierarchical mesocarbon microbeads as the precursor, delivering good electrochemical behaviors both in LIBs and SIBs.[106]

4.1.2 Pre-oxidation method.
Another pre-treatment method for HC precursors is the pre-oxidation process, as reported by Wu and coworkers. A self-supporting HC paper derived from tissue was rationally designed and prepared as a practical additive-free anode for room/low-temperature SIBs with a high ICE (Fig. 6h).[105] The as-prepared electrode delivered an ultrahigh ICE of about 91.2% with excellent energy storage performance in terms of outstanding high-rate capability (Fig. 6i and j), exceptional cycle stability and desirable low-temperature behaviors in ether electrolyte (Fig. 6k and l). Furthermore, the systematic analysis also exhibited that the sodium storage mechanism is an "adsorption–intercalation" process and the plateau region was the rate-determining step for the as-prepared electrode with lower electrochemical reaction kinetics, which could be significantly promoted. Additionally, according to Shi and coworkers, a 3D "overpass" hierarchical porous carbon membrane (PMP) was gained by pre-oxidation treatment at 250 °C for 2 h in air, followed by a carbonization process at 1100 °C for 2 h.[59] It was stated that
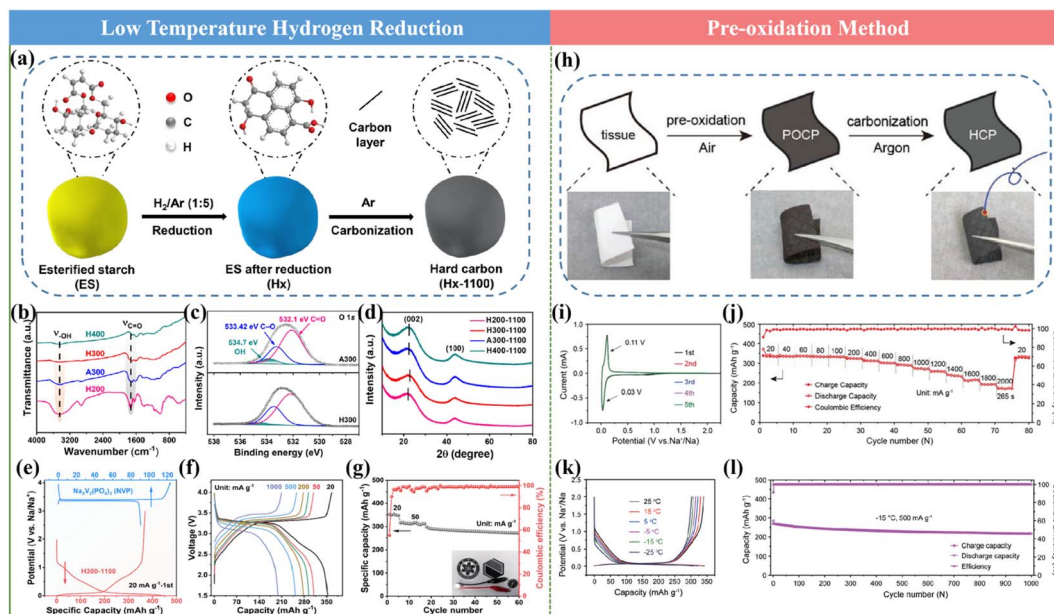
Fig. 6 (a) Diagram of the process for the fabrication of Hx-1100. (b–d) FTIR spectra, high-resolution of O 1s spectra of A300 and H300, and XRD patterns of different samples. (e–g) Electrochemical behaviors of H300-1100//NVP full cells. (h) Diagram of the preparation process of HCP and the digital photos of tissue, POCP and HCP. (i and j) CV curves and rate behaviors of HCP anode, (k) GCD curves at various temperatures under 50 mA g^{-1} and (l) cycling performance under 500 mA g^{-1} at $-15\ ^{\circ}\text{C}$.

this pre-oxidation treatment provided a favorable structural stability effect in the preparation procedure. Specifically, the formation of a channel-skeleton coupling microstructure in the optimal sample PMP-5 promoted the wettability of the electrolyte, improved the electron/ion transport, and boosted the Na storage property comprehensively. Particularly, when evaluated as a free-standing anode, it showed superior cycling stability with about 91% capacity retention over 300 cycles at 0.5C and an extremely high ICE of about 90.5% could be achieved. More significantly, a full-cell fabricated with the layered O3-Na(NiFeMn)$_{1/3}$O$_2$ cathode exhibited a superior energy density of about 287 W h kg^{-1}, remarkable rate behavior and advanced cycle stability. This research offers a possible approach to enhance the Na storage performance of HCs by membrane science and pore engineering. Besides, it is worth noting that oxygen functional groups can be successfully introduced through the pre-oxidation process, resulting in the formation of extensive cross-linking structures and destroying the degree of graphitization, which are essential for the modification of soft carbon and the corresponding work was reported by Hu *et al.* and other researchers.[28,29]

4.1.3 Chemical activation strategy. Tuning the pore configuration and microcrystalline state of the microstructure of coal during thermal transformation plays a vital role in promoting its Na$^+$ storage behavior. The strategy of converting the nanopores with open features and ordered carbon crystallite into closed pores surrounded by short-range ordering micro-structures through chemical activation, and subsequently high-temperature carbonization process was developed by Zhao and coworkers.[107] Significantly, these specific microstructures had a dominant contribution to the reversible capacity in the low-voltage plateau region, which delivered a high specific

capacity of about 308 mA h g^{-1} for a half-cell and $231.2 \text{ W h kg}^{-1}$ for a full-cell. Furthermore, the optimal electrode material also exhibited a superior supercapacitive performance when constructed with activated carbon electrode. This report offers valuable guidance for the rational regulation of closed pore microstructures in HCs for energy storage devices.

4.1.4 Template-assisted pore regulation method. The template-assisted method for pre-treatment has been proven to be an effective way for promoting the specific capacity of the resultant HCs. Remarkably, HCs with an extraordinary advanced capacity of about 478 mA h g^{-1} was reported by Komaba and coworkers by carbonizing a freeze-dried mixture of glucose and magnesium gluconate *via* an MgO-template approach.[67] Through a pre-treatment process at $600\ ^{\circ}\text{C}$, MgO particles with a nanosize structure could be generated inside the carbon matrix, and subsequently after an acid leaching procedure for MgO, followed carbonized at $1500\ ^{\circ}\text{C}$, the resultant HC anode materials showed nanoporous structures with a large specific surface area of about $484 \text{ m}^2 \text{ g}^{-1}$. This was elucidated by first principles molecular dynamics calculations and further observed from TEM images. Additionally, a large total volume derived from the formed nanopores (or nanovoids) and surrounding thin graphitic layers with desirable interlayer spacing distance were also generated, significantly exhibiting an influence on the Na storage in HCs. Furthermore, the correlation between nanostructures and synthetic conditions on the electrochemical properties of HCs in SIBs was systematically investigated. The optimal sample presented a high ICE of about 88% in a half-cell system; besides, a remarkably high energy density of about 358 W h kg^{-1} was achieved in a full-cell with P2-Na$_{2/3}$Ni$_{1/3}$Mn$_{1/2}$Ti$_{1/6}$O$_2$ as the positive electrode owing

to the advanced HC anode, demonstrating its great potential for practical application in SIBs. Another interesting work using the freeze-drying method and further carbonization at 1000 °C to acquire graphene/hard carbon spheres (GHSs) was proposed by Song *et al.*[68] The general multi-interface strategy with massive ingenious internal interfaces between the carbon matrix and crystalline graphene in HC spheres can serve as a pathway for gas escape during the pyrolysis of sucrose, thus avoiding the formation of abundant pores. The N_2 adsorption measurements showed that the resultant material with a high packing density of 0.910 g cm^{-3} possessed a relatively low specific surface area of 13.3 m^2 g^{-1}. Moreover, this unique structure also can offer highly conductive pathways for ion and electron transportation. Subsequently, the electrochemical behaviors of the electrode applied in LIBs and SIBs in terms of reversible capacity, rate capability and low-temperature performances comprehensively improved, indicating its promising commercialized prospect for practical applications.

4.1.5 Spray drying method. Besides the freeze-drying method for pretreatment, spray drying is also employed. In an interesting work, a series of HC near spheres (HCNSs) were designed by Jiang and coworkers by spray drying and subsequent direct pyrolysis in a wide range temperature, which is aimed at addressing the issue of the ambiguous correlation between the Na storage behavior and microstructure of HCs.[63] Accordingly, the results exhibited that the discharge capacity of the plateau region can be attributed to the Na$^+$ insertion process in the long-range ordered carbon structure inside HC. In contrast, the discharge capacity of the slope region can be ascribed to the Na$^+$ adsorption on the surface of HC. Particularly, with a suitable interlayer distance (>0.364 nm), the "plateau capacity" can be effectively enhanced, and simultaneously the total Na-storage capacity improved. At the same time, increasing the specific surface area will result in a high "adsorption capacity" at high potential. As a result, the optimized sample prepared at 1200 °C with an interlayer distance of about 0.372 nm, suitable L_c value, specific surface area of about 5 m^2 g^{-1}, $I_D/(I_G + I_D)$ of about 0.70 and the ratio of sp^2 area to sp^3 area from C 1s of about 1.85 presented a desirable reversible capacity of about 305 mA h g^{-1} with a slope capacity of about 135 mA h g^{-1} and plateau capacity of about 170 mA h g^{-1}. Another simple preparation strategy was developed to prepare graphene-coated low-surface-area HC carbon microspheres (HCG) by Shi and coworkers by spray drying-direct pyrolysis at 120 °C and 900 °C.[62] Specifically, SEM and TEM showed that the as-prepared material possessed a 3D conductive network and ordered microcrystalline structure. Meanwhile, abundant mesopores were detected in the N_2 adsorption measurement. Benefitting from its unique microstructure, HCG delivered an excellent electrochemical performance in SIBs as well as PIBs with fantastic energy densities (240 and 210 W h kg^{-1}). Significantly, due to the larger diffusion coefficient and higher insertion potential in the plateau region, the kinetic analysis illustrated that the rate capability of HCG in PIBs was better than that in SIBs. Additionally, similar mechanisms for the energy storage process of Na and K were also proposed in HCG.

4.1.6 Template-assisted catalytic strategy. It was demonstrated that the methods applied in previous research, including increasing the carbonization temperature and decreasing the heating rate in a normal way, created more short-range-ordered microstructures in HCs.[98] Accordingly, a more advanced strategy is needed to create HCs with less defects, large size, and higher levels of internal ordered microstructures to promote the Na storage performance. Recently, the template-assisted strategy seems to be an effective method to address the above-mentioned issues, certainly showing remarkable achievements. For example, Liu and coworkers employed an external graphite template for the growth of graphite crystals at 1300 °C and realized the low-temperature graphitization effect.[108] The as-prepared HCs with high-level ordered structure within the pseudographitic domains were successfully achieved. Besides, a desirable ICE, high reversible capacity and fantastic cycle stability were achieved. Additionally, the full cell assembled with Prussian blue as the cathode and the as-prepared HC anode exhibited a discharge capacity of about 256 mA h g^{-1} and excellent cycling behavior with 82% capacity retention after 100 cycles. Afterwards, the same group reported another study using the same strategy, applying cotton as a precursor to realize large-area graphite-like crystals inside the HC microstructure. The large interlayer spacing inside the perfectly parallel stacked carbon layers was beneficial for the reversible intercalation and deintercalation of Na$^+$, achieving a dramatically advanced ICE of 95% and specific capacity as commercial graphite applied in LIBs.[109] Besides the graphite-assisted template, another example of the graphene-inducing graphitization strategy using a phenolic resin precursor was reported recently by Huang and coworkers.[110] The formation mechanism elucidated that high temperature would lead to the arrangement of the aromatic ring in the carbon precursor along the graphene layer because of the hydrogen bonding interaction effect (as presented in Fig. 7a–c), which can be estimated from the Raman and XPS measurements and the transition of hybridization carbon from sp^3 to sp^2 state can be detected. Meanwhile, fewer defects and lower specific surface area are delivered under this treatment. These unique characteristics of microstructure undoubtedly bring in remarkable electrochemical performance regarding half-cells and full-cells. The special microstructure of graphite-like crystals can provide more possibilities for exploring new properties and applications.

4.1.7 Liquid template-assisted activation strategy. Another significant work on the template strategy is the liquid-template assisted activation strategy reported by Wang and coworkers (as presented in Fig. 7d).[111] Specifically, employing rosin as the precursor *via* liquid salt template-assisted and potassium hydroxide dual-activation treatment, a special N-doped HC with an "egg puff"-like structure was successfully prepared (Fig. 7e–g), which showed great promise for improving the solid diffusion dynamics and preventing side-reactions during the Na metal plating process (Fig. 7h). The electrical performances exhibited that the optimal anode in ether-based electrolyte possessed an ultrahigh ICE of about 92.9%, specific capacity of about 367 mA h g^{-1} at 0.05 A g^{-1} and 183 mA h g^{-1} even at 10 A g^{-1}. Furthermore, it also delivered outstanding cycling
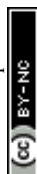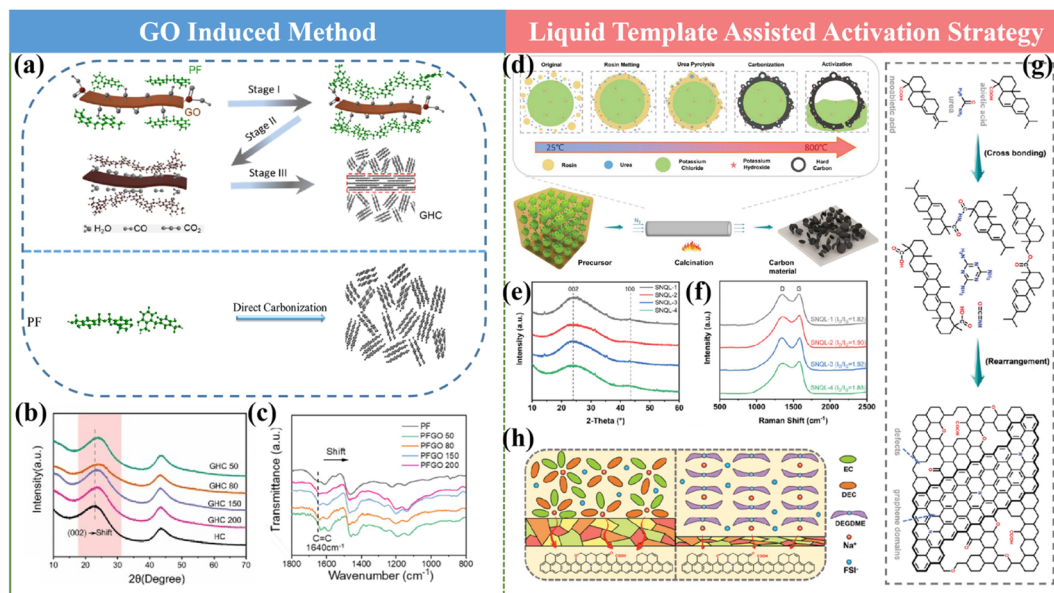
Fig. 7 (a) Proposed formation mechanism of GHCs under different conditions, (b and c) XRD patterns and FTIR spectra of GHCs, (d) diagram for the preparation of "egg puff"-like HC, (e and f) XRD patterns and Raman spectra of SNQLs, (g) diagram of the structure transformation and (h) diagram of SEI in different electrolytes.

behavior with 151 mA h g^{-1} after 12 000 cycles at 5 A g^{-1}. This finding will certainly offer an effective approach for achieving HC anodes with advanced rate performances.

4.1.8 Metal catalysis strategy. To decrease the challenging degree of graphitization in HCs, other external conditions can also be effectively employed, *e.g.*, metal ion-assisted catalytic carbonization. For instance, Fe-catalyzed phenol-formaldehyde resin-derived HC was prepared by Goodenough and coworkers at a relatively low temperature of 800 °C for 4 h.[112] This is a significant work to achieve long-range ordered microstructures in HC by adopting the ion-catalyzed effect at a low temperature, as confirmed by Raman spectroscopy and TEM images. The formation mechanism of expanded nanographite and micropores inside the HCs can be ascribed to the fact that Fe converts the state of sp^3 carbon to sp^2 and the free rearrangement of disordered graphene sheets into expanded nanographite becomes feasible. As a result, due to the merits of the structural features, the HCs showed an excellent Li/Na storage performance. Interestingly, the element of Ni also displayed a similar effect as Fe and Zhao's group fabricated N-doped HC nanoshells by prechelation between Ni^{2+} and chitosan.[56] Unfortunately, their Na storage behavior was far from favorable. Moreover, Zhang and coworkers also reported the preparation of novel hierarchical hollow HC spheres at an even lower temperature of about 600 °C *via* the Ni-catalyzed graphitization technique and an ICE of about 86% was obtained.[113] Although a metal-ion catalyst can effectively improve the degree of graphitization at a relatively low temperature, there is much space to promote the electrochemical behaviors of the as-prepared HCs in SIBs. Another CVD-like method with Mg catalysis reaction to prepare hybrid-structured HC integrated with carbon nanosheets and carbon nanotubes was facilely developed at 600 °C.[114] Given the features of the above-

mentioned two compositions, the microstructures in terms of defects, specific surface area and nanovoids could be regulated through the synthetic temperature, which greatly contributed to the slope-dominated specific capacity. The desirable sample prepared at 600 °C presented the optimal Na storage performance with a high specific capacity of about 390 mA h g^{-1}, and good cycle behavior of about 76.92% after 100 cycles at 0.05 A g^{-1}. The detailed calculation from the electrochemical measurements exhibited that this electrode possessed a capacitive-controlled mechanism related to the slope-dominated storage behavior with fast reaction kinetics, accounting for its excellent rate capability. The full-cell with the-obtained Na$_3$-V$_2$(PO$_4$)$_3$@C cathode showed a good Na storage performance, illustrating its practical application in SIBs.

Motivated by the previous reports and to solve the existing issues, recently, our group proposed metal ion-assisted catalytic carbonization based on a flexible paper towel precursor (Fig. 8a and b), in which various metal ions including Na$^+$, Cu^{2+}, Ni^{2+}, Co^{2+}, Fe^{3+} and Mn^{2+} metal chlorides with different concentrations were employed.[71] By tuning the types of metal ions and their concentrations, the micropore size and interlayer spacing of the graphite microcrystalline could be controllably regulated (Fig. 8c and d). Specifically, the TEM images showed that Mn^{2+} ions with a moderate concentration could precisely tune the graphitization degree to grow long-order graphene layers. In contrast, the HCs with a high concentration of metal ions exhibited over-graphitization features, and subsequently blocked the accessible channels of Na$^+$. Furthermore, Mn^{2+} can break the sp^3 carbon bridge between graphene sheets at high temperatures, leading to the rearrangement of the graphene sheets, which resulted in the formation of nano-graphite domains and micropores.[115] Moreover, the interaction between oxygen and metal ions with this special treatment
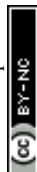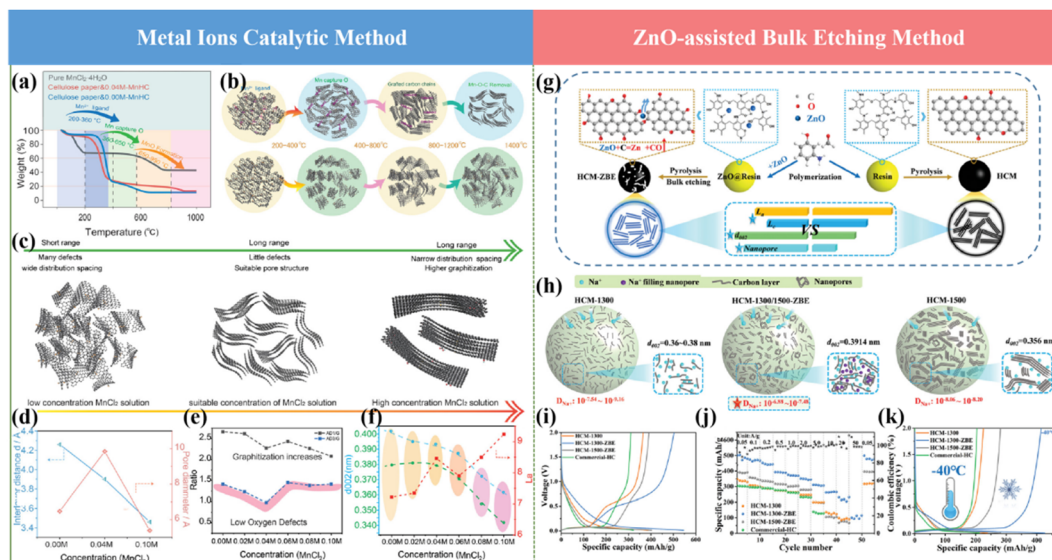
Fig. 8 (a) TG curves of various HCs under various catalytic conditions. (b) Illustration of HC pyrolysis process tuned by manganese ion. (c) Illustration of change in the carbon layer with manganese salt concentration. (d) Relationship of interlayer distance and pore diameter with manganese salt concentration. (e and f) Changing trends of A_{D1}/A_G, A_{D3}/A_G, d_{002} and La at various $MnCl_2$ concentrations. (g) Illustration of the synthesis route of the samples. (h) Diagram of Na^+ diffusion in HCM-1300/1500 and HCM-1300/1500-ZBE. (i–k) Electrochemical performances of various samples.

could also facilitate the removal of the irreversible oxygen-enriching defects (Fig. 8e and f). As a result, an ultrahigh reversible specific capacity of about 336 mA h g^{-1} and a satisfactory ICE of about 92.05% were successfully delivered. A more detailed Na storage mechanism regarding the "adsorption–intercalation–pore filling-sodium clusters formation" process in the as-obtained HCs was also reported. The novel metal element doping strategy can realize both a high ICE and high reversible specific capacity compared with the non-metal doping route. Further, this significant work is of great importance for the development of high-performance HCs for SIBs.

It is a well-established fact that the rate capability of SIBs is crucial for their practical applications. Thus so far, significant efforts have been devoted to introducing more defects or porosity in the microstructures of HC anode materials to promote their rate capability.[116] Unfortunately, the overall performances of SIBs are still unsatisfactory regarding their low ICE and low plateau capacity when adopting these approaches. Based on this, Zhao and coworkers constructed a well-regulated structure with ultrafast Na$^+$ storage behavior in the range of 0.01–2 V through a ZnO-assisted bulk etching approach, as shown in Fig. 8g.[117] The coefficient for Na$^+$ diffusion improved by 2 orders of magnitude and the correlation between the electrochemical performance and electronic structure of HCs was established (Fig. 8h). More importantly, the Na storage mechanism in HCs was proved *via* comprehensive *in(ex) situ* techniques, indicating the co-existence of interlayer Na$^+$ intercalation and nanopore Na filling process below 0.1 V. Due to the merits of microstructures including high specific surface area, high content of oxygen, optimal graphic layers and interlayer spacing distance, unprecedented electrochemical performances have been delivered in terms of extremely high specific capacity of about 501 mA h g^{-1} at room

temperature, 426 mA h g^{-1} at −40 °C, and extraordinary advanced rate capability of 107 mA h g^{-1} even at a high current density of about 50 A g^{-1} (Fig. 8i and k).

Besides the aforementioned investigations, an HC anode with atomically incorporated zinc single atoms to regulate its bulk and surface microstructure was also proposed by the same group recently.[118] The optimal HC sample with reduced defect content, highly developed nanopores (diameter of ≈0.8 nm) and expanded graphite regions (d_{002} = 0.408 nm) exhibited exceptional Na$^+$ storage behavior. The as-prepared Zn–N$_4$–C architecture in the HC matrix can be beneficial for catalyzing the decomposition of NaPF$_6$ and formation of a thin and inorganic-rich SEI, which will lead to fast interfacial Na$^+$ storage kinetics. The overwhelmingly high reversible capacity of the as-obtained HC anode of about 546 mA h g^{-1} at room temperature and 443 mA h g^{-1} at −40 °C was achieved. More importantly, an outstanding rate capability of about 140 mA h g^{-1} at 50 A g^{-1} was delivered, outperforming the state-of-the-art electrochemical performance in SIBs. When fabricated with an NVP cathode, a high energy density of about 323 W h kg^{-1} was exhibited at a power density of about 7.02 kW kg^{-1} (based on the total active mass in both electrodes). These findings can eventually provide new opportunities for constructing advanced HCs and applying them in sustainable energy storage systems.

Generally, to be used in large-scale production, the pretreatment processes for HC materials need to meet certain requirement considerations: firstly, they should possess low energy consumption characteristics, and secondly, effective realization of structural regulation of the raw material should be achieved. Lastly, whether the products from pretreatment process have an effect on the equipment used for the high temperature carbonization step should be considered.

4.2 Advanced high-temperature carbonization method

In recent years, ultrafast heating methods including Joule heating, multifield-regulated spark plasma sintering (SPS), and microwave heating have been utilized to develop novel carbon anode materials, clarifying special and often advanced behaviors compared with the conventional heating strategies. These unique methods have also opened excellent opportunities for material synthesis and exhibited extraordinary application potential in supercapacitors, fuel cells, catalysis, batteries, lighting devices, waste recycling, sensors, *etc.* In this section, the recent research on producing novel HCs by ultrafast heating methods are summarized, and their advantages and limitations are also described.

4.2.1 Joule heating. HCs represent carbon materials that cannot be transformed into graphite at high temperature, which are commonly derived from sugars, biomass, or polymers *via* direct heating or hydrothermal carbonization, followed by a further pyrolysis treatment at 1000–1873 K.[40] They are regarded as the most promising anode materials for SIBs. Given its merits of scalable, efficient, and rapid features, Joule heating has been widely used in rapid heat treatments and material preparation process.[119–121] Joule heating is an electrothermal approach that has the potential to reach a temperature of more than 3100 K within milliseconds. It seems to offer some environmental benefits due to the fact that it does not involve the use of toxic chemicals and provides a new valorization route for various wastes, most of which are landfilled or littered. As reported, Joule heating processes have been employed to synthesize various nanomaterials with interesting structures and compositions, such as high-entropy alloys and turbostratic graphene. Furthermore, it can be used as a simple rapid heating method to kinetically trap volatile products of interest and study their evolution based on the peak temperature or reaction duration.[119] Specifically, it also have been considered as a specific method in recent research to produce HCs. Also, some recent groundbreaking research provided novel research directions for producing HCs for SIBs through this method. In this respect, Hu and coworkers applied switchgrass as a biomass example and carbonized it at a high temperature of greater than 2000 °C *via* the tailored Joule heating process for SIB applications, as shown in Fig. 9a.[70] An ultrahigh temperature of about 2050 °C resulted in superior electrical conductivity and highly ordered pseudographite structure with an interlayered spacing of about 0.376 nm, which were beneficial for achieving a significant Na^+ storage property (Fig. 9b–d). Compared to the sample prepared at 1000 °C, the switchgrass prepared under 2050 °C exhibited an apparently enhanced ICE (Fig. 9e and f). Meanwhile, this HC anode showed an excellent rate capability due to its improvement of electrical conductivity. Furthermore, an outstanding cycling performance of up to 87% capacity retention after 800 cycles was also achieved. Afterwards, they proposed a new idea to obtain highly crystalline graphitic carbon from lignin-based biomass by employing the same Joule heating process.[122]

4.2.2 SPS method. Lately, Titirici and coworkers utilized the emerging SPS method to prepare HC *via* a high speed and boosted pyrolysis process, as presented in Fig. 9g and h.[123] Significantly, lower porosity, smaller surface, fewer defects and lower oxygen content could be realized compared to that pyrolyzed in a traditional way, as detected from the N_2 adsorption, XRD (Fig. 9i), Raman, XPS results. Remarkably, the accelerated
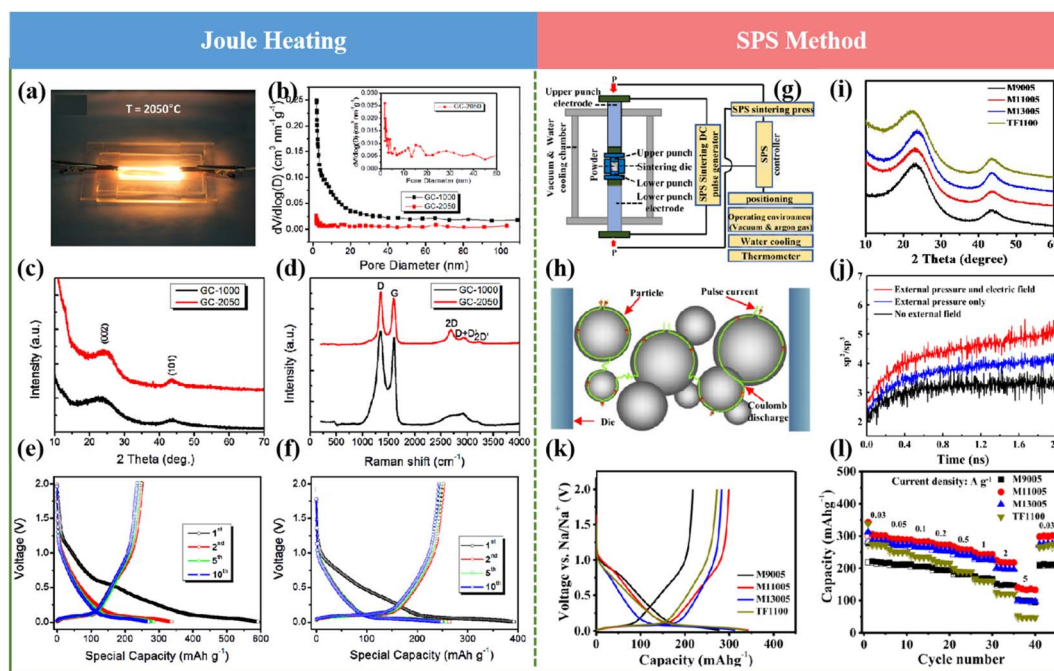

Fig. 9 (a) Photograph of switchgrass-derived HC *via* Joule heating. (b–d) Pore size distribution curves, XRD patterns, and Raman spectra of GC-2050 and GC1000. (e and f) Charge−discharge curves of GC-2050 and GC1000, (g) diagram of the SPS system, (h) annealing mechanism, (i) XRD patterns of HCs, (j) change in the structural composition of the materials and (k and l) electrochemical behaviors of HCs.

pyrolysis mechanism from the quickly increased carbon sp^2 content under the multifield effect was elucidated by molecular dynamic simulations (Fig. 9j). Accordingly, the as-obtained HCs displayed noticeably promoted kinetics and Na storage capacity compared to the HCs derived from the traditional route (seen in Fig. 9k and l). Impressively, many conspicuous advantages including ultrahigh heating and cooling speeds, high heating treatment at a specific location with little change in the original structure of the precursors, and significantly reduced energy consumption have been exhibited from Joule heating. However, this high-temperature carbonization method demands high-quality instruments and equipment. Thus so far, the investigation devoted in this field is limited. Consequently, strengthening the reports related to this technique is crucial to commercial development and creating novel HCs in SIBs.

4.2.3 Microwave heating. Besides Joule heating treatment, another simple and efficient synthesis method of microwave heating at a high pyrolysis rate of about 100 °C min^{-1} at low temperature (700 °C, 800 °C, and 900 °C) was reported recently by Yang and coworkers.[124] In this study, industrial waste plastic was selected as the precursor to prepare HCs with different micromorphologies. Particularly, the relationship between the microstructure and electrochemical properties was also evaluated. The N_2 adsorption and TEM pore analysis showed that MW-900 possessed a large number of closed pores and a reversible discharge capacity of about 344 mA h g^{-1} could be achieved. Moreover, based on theoretical calculations with Matlab, XRD, *in situ* Raman and *ex situ* XPS measurements, an Na$^+$ storage mechanism based on adsorption–intercalation and pore-filling process was proposed. This finding can offer guidance for designing high-performance anode materials in energy storage devices.

In conclusion, advanced high-temperature carbonization methods exhibit the ability to reach extremely high temperatures with rapid heating and cooling rates and increase the efficiency and decrease the heat loss, resulting in low energy consumption. However, some limitations and challenges should be considered in large-scale production processes. Firstly, all ultrafast heating strategies face difficulties in precise measurement and controlling the reaction temperature. Secondly, it still remains a challenge to establish a correlation between the synthetic conditions or parameters during the ultrafast heating process and the structure of the obtained HCs, which precludes the rational and controllable synthesis and design of HCs. Finally, safety factors should be considered.

4.3 Advanced post-treatment method

Besides the previously mentioned pre-treatment and direct carbonization strategy to acquire high-performance HCs, in recent years, it has been found that post-treatment is also an effective method to obtain superior-performance HCs. Generally, some synthesized HCs are used to prepare electrodes and adopted in energy storage systems directly, but there are many reports including the post-treatment of the electrode materials and the multilayer coating for electrodes, which display an enhancement in electrochemical performance. In this section, some advanced post-treatment methods are summarized.

4.3.1 CVD strategy. According to the reported mechanism of the Na storage process, the pore structure, as one of the most important components inside the HC microstructure, plays an essential role in the electrochemical performance for SIBs. Besides the aforementioned pore closing method and pore-forming strategy under high temperature treatment, sieving carbon (SC) with tightened pore entrances proposed by Yang and coworkers through chemical vapor deposition (CVD) with methane was proven to be another effective strategy to obtain high-performance HCs, as shown in Fig. 10a.[65] The resultant SC anode material with a decreased specific surface area inevitably suppressed the formation of an excessive SEI film (Fig. 10b), which could be inspected through SAXS analysis (Fig. 10c). As a result, the ICE was evidently improved from 16% to 81%. Moreover, Na clusters emerged inside the nanopores; meanwhile, regulating the body diameter of the nanopores achieved a high reversible capacity originating from Na cluster formation, and consequently an extraordinary high specific capacity of about 430 mA h g^{-1} was delivered. Specifically, the precise progress of the Na clustering process from Na ions to the formation of Na clusters could be observed from the theoretical calculation, and four types of distinct Na groups existed according to the different Löwdin charges and carbon environments, elucidating the different interactions between carbon and Na. Hence, the achievement of the modification of the nanopores exhibited the great potential development of porous carbons for practical anode applications. After that, by using the CVD method, Xie and coworkers designed and prepared HCs coated with a homogeneous curly graphene layer (HC-CG) without catalysts.[125] In this unique construction, the graphene layer coating not only shielded the surface defects of HCs but also enhanced their electronic/ionic conductivity, resulting in a desirable ICE of about 89.3%. At the same time, the curling structural features of graphene layer led to the formation of numerous micropores with additional active sites, achieving a high specific capacity of about 358 mA h g^{-1}. In particular, an outstanding rate capability and excellent cycle stability were also obtained. This research offers an easy defect/microstructure regulation approach for HCs and deepens the understanding of the mechanism for Na storage in the plateau region.

However, until recently, few strategies have focused on the modulation of microstructural systems for the simultaneous construction of graphite-like structural domains and microporous structures in bulk carbon. In this regard, Cao and coworkers firstly proposed a space-confined chemical vapor deposition approach to fill graphitic-like carbon domains into the micropores of commercial activated carbon to form filled HCs with tunable microstructures.[126] By tuning the preparation condition, the micropores of the filled carbon, size of the graphitic carbon domains and interlayer spacing of graphitic carbon could be effectively regulated. Impressively, the as-obtained filled carbon exhibited outstanding electrochemical performances in LIB, SIB and PIB devices. Specifically, an ultrahigh specific capacity of about 435.5 mA h g^{-1} and
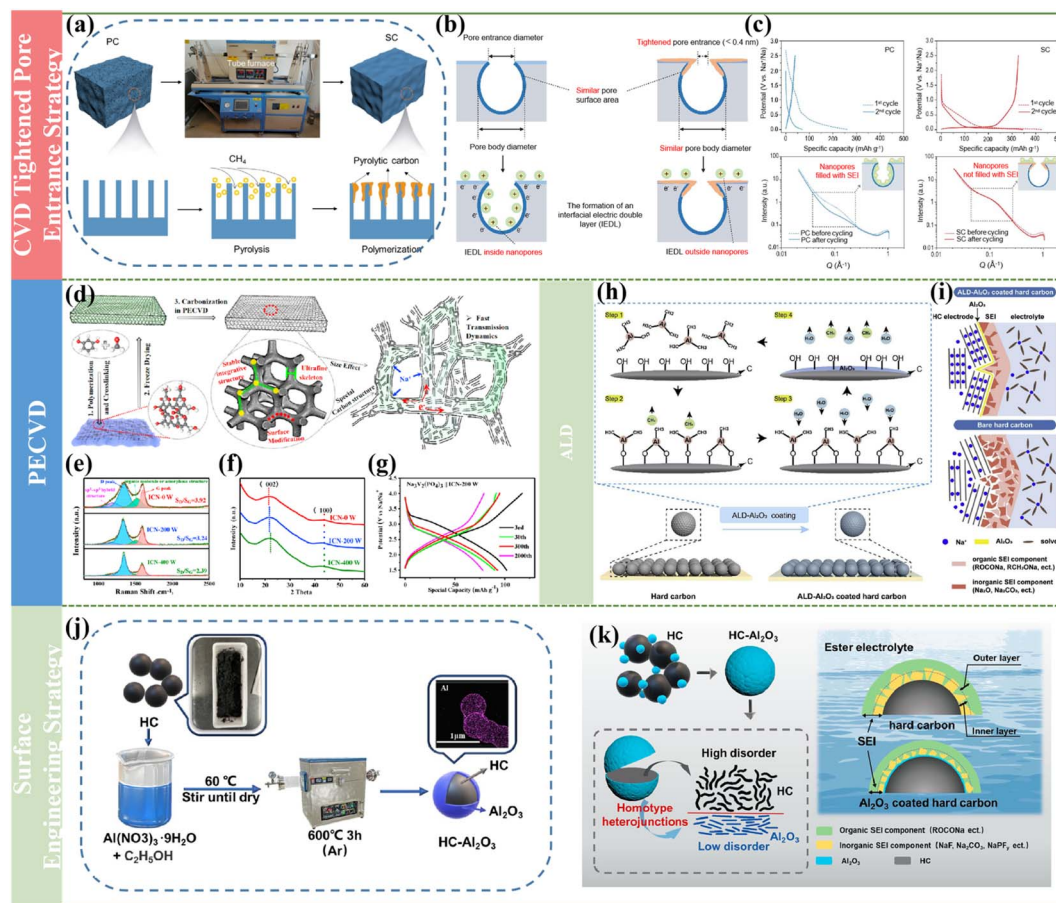
Fig. 10 (a) Process for the preparation of sieving carbons *via* CVD. (b) Illustration of a typical porous carbon (left) to produce sieving carbon (right), and the corresponding IEDLs. (c) Charge/discharge curves and SAXS patterns of PC and SC anodes, and inset: the relative location of the SEI to the nanopores. (d) Diagram of preparation process for integrative carbon network (ICN). (e and f) Raman spectra and XRD patterns of ICN-X. (g) Charge−discharge curves for $Na_3V_2(PO_4)_3$//ICN-200 W full battery. (h) Illustration for depositing Al_2O_3 on the surface of HC *via* ALD process. (i) Influence of ALD-Al_2O_3 coating on HCs. (j and k) Diagram of Al_2O_3 layer coating preparation process and improving the ICE of the HC electrode.

desirable cycle behavior with 80% capacity retention over 1000 cycles could be achieved for SIBs. Furthermore, the microstructures and electrochemical properties of the filled carbon prepared from various carbon substrates and carbon sources were systematically investigated. It was determined that it is favorable for large-scale production when benzene and its derivatives are applied as the carbon sources, which can be ascribed to the fact that the as-obtained carbon materials exhibited moderate sodium storage capacity but high ICE, and the as-prepared materials were easy to control due to the saturation deposition and slow deposition rate. This significant work can offer a practical approach to engineer commercial carbon materials to construct advanced HCs for high-performance alkali metal-ion batteries.

4.3.2 Plasma-assisted method. Owing to the fact that electrochemical reactions take place on the electrode/electrolyte interface, the surface chemistry of HC anodes is crucial in energy storage systems and valid measures for surface modifications are urgently needed. Based on this, Xie and coworkers proposed a low-temperature oxygen plasma treatment strategy with non-destructive feature for tailoring the surface chemistry of commercial HC.[127] According to the Raman and XRD results, the resultant optimal electrode material showed a low defective surface and highly ordered structure with no obvious change in layer spacing, which undoubtedly favored the process of Na^+ de/insertion and helped to reduce the corresponding side reactions. Besides, XPS revealed that oxygen functional groups (C=O) were generated on the surface of HCs under this treatment, creating more active sites for Na^+ storage. Because of the regulation of its microstructure, the as-prepared optimized HC presented a significant improvement in ICE from 60.6% to 80.9%. Also, a desirable specific capacity and excellent rate capability were exhibited. This finding can offer a possible route to regulate the surface chemistry for the construction of high-performance HCs in energy storage devices. Inspired by the above-mentioned study, accurately tuning the functional groups especially oxygen-containing functional groups in the HC precursors is another meaningful way to obtain a satisfactory Na storage performance. In fact, the correlation between the influence of original oxygen-containing groups inside in precursor on the

final microstructure and Na storage behavior is not clear yet to date. Thus, Hu and coworkers conducted very interesting research applying anthraquinone derivatives as precursors with different oxygen-containing functional groups to prepare different disordered carbon anodes for SIBs.[128] This significant work can offer valuable guidance for the rational regulation of the functional groups inside HCs for high-performance SIBs.

Another feasible and rapid method of the plasma-assisted chemical vapor deposition process was proposed at a relatively low carbonization temperature (900 °C) by Li and coworkers.[66] As a consequence, a novel integrative carbon network material (ICN) was successfully prepared on a large scale, as presented in Fig. 10d. Significantly, surface plasma treatment can effectively control the content of –C=O groups, interlayer spacing and order degree of surface carbon stacking layers, which were further confirmed by XPS, XRD and Raman measurements (Fig. 10e and f). Accordingly, all-round improvements were exhibited for the optimal sample (content of –C=O groups of about 39.7% and d_{002} of about 0.367 nm), including an extremely high specific capacity of about 389.5 mA h g^{-1}, excellent rate performance (285 mA h g^{-1} at 2000 mA g^{-1}), and excellent cycle behavior (72.2% over 10 000 cycles). The dynamic analysis illustrated that the capacitive mechanism for Na$^+$ rapidly inserting/adsorbing with the surface/subsurface atoms mainly led to the improved Na storage behavior. The full-cell assembled with an NVP cathode could successfully light a diode with ultra-high rate capability, indicating its potential for practical application (seen in Fig. 10g). These findings shed light on the microstructure regulation of long-life performance HCs in SIBs. Furthermore, the plasma-assisted method will be more widely used for material preparation if the regulation of functional group homogeneity can be achieved.

4.3.3 Coating approach. HC anode materials, especially their properties on the surface, also have a significant impact on the solid electrolyte interface (SEI), and subsequently affect the electrochemical performance of the energy storage devices. Research on LIBs showed that the thickness of the SEI film formed on the edge plane of the graphite anode is several times higher than that on the base plane, and the chemical composition on the surface of the anode material can inevitably change the film-forming potential of the SEI layer, and followed the influence of its chemical connection with the surface of the electrode, thereby affecting the ion transportation and interfacial charge transfer of the SEI interfacial process.[129] Based on this, Sun et al. used an extremely thin layer of Al$_2$O$_3$ deposited on the surface of Na as an artificial SEI film, and they found that the Al$_2$O$_3$ layer could not only inhibit the production of Na dendrites, but also affect the thickness and composition of the SEI film.[130] Very recently, Cao and coworkers reported the direct atomic layer deposition (ALD) of an ultrathin Al$_2$O$_3$ layer on the surface of HCs in SIBs (shown in Fig. 10h), which showed that the real thickness of the as-prepared HC with 20 ALD cycles (SHC-ALD20) reached up to 2.1 nm by accurately depositing an Al$_2$O$_3$ layer on a silicon wafer, indicating a thickness of about 0.105 nm per ALD cycle during the Al$_2$O$_3$ layer deposition process.[131] This is consistent with the thickness evaluated from the TEM analysis (about 2.2 nm). Moreover, the specific surface area of SHC-ALD20 also decreased from 385 m^2 g^{-1} for the uncoated anode to 331 m^2 g^{-1}, with a simultaneously decrease in the total pore volume from 0.212 cm^3 g^{-1} to 0.179 cm^3 g^{-1}, demonstrating that the inner pores of HCs can be filled by Al$_2$O$_3$ to some extent, but not the whole nanopores because of the limited dangling bonds (C–O–H) and steric hindrance. The results clarified that the Al$_2$O$_3$ film can serve as an "artificial SEI" on the HC anode surface (presented in Fig. 10i), efficiently suppressing the decomposition of the electrolyte and subsequent high ICE (75%) and cycle performance (90.7% capacity retention after 150 cycles) with the optimal thickness of 2 nm. Furthermore, the deposited Al$_2$O$_3$ layer could effectively reduce the electrode overpotential and interfacial resistance, resulting in an increased reversible capacity of about 355 mA h g^{-1}. With the precise regulation of the thickness of the coating layer by the ALD method, research can offer guidance for the surface modification strategy to promote the interface stability of HCs for high-performance SIBs.

In contrast to the expensive equipment required for the ALD method, another convenient and versatile surface engineering way to improve the ICE was reported by Wu et al. By constructing a stable homo-type amorphous Al$_2$O$_3$ layer through a normal hydrothermal treatment coating approach (Fig. 10j), the as-prepared HC material showed a decreased specific surface area of 6.91 m^2 g^{-1}.[132] Meanwhile, the value of I_D/I_G decreased with an increase in Al$_2$O$_3$ content in the Raman spectra, demonstrating that the Al$_2$O$_3$ coating layer is beneficial for reducing the content of active sites and defects in HCs. Additionally, an ultrathin Al$_2$O$_3$ coating layer of about 4 nm with a lower disorder degree was expected to suppress excessive side reactions, which could reduce the irreversible Na adsorption, and subsequently improve the ICE (from 64.7% to 81.1%) for HC (Fig. 10k). More interestingly, the full cell device assembled with the resultant HC electrode also exhibited much better electrochemical behaviors, indicating that this straightforward surface modification method can significantly boost the practical application of high-performance SIBs.

Furthermore, kinetically controllable coating technology is a highly controllable liquid-phase coating method emerging in recent years. By accurately tuning the kinetic parameters of the coating process, the coating layer can be uniformly and controllable deposited on the surface of the electrode materials to prepare a uniform nanoscale coating layer.[133] Compared with physical methods such as the aforementioned ALD and magnetron sputtering, it exhibits outstanding advantages such as simple process, low cost and easy magnification features. For example, Wan et al. used this technique to control the deposition dynamics by adjusting the initial pH and using urea as a sustained release agent, and a 10–90 nm-thick AlPO$_4$ layer was successfully deposited on the surface of LiCo$_2$O$_3$, greatly improving the recycling performance of the material.[134] Surface coating can efficiently regulate the surface properties of materials without affecting the internal structure. Kinetic controllable coating technology can also be applied to HCs, which cannot affect their internal structure and characteristics, thus maintaining a high capacity, and has great potential in the regulation of surface characteristics such as specific surface area, chemical composition and structure.

4.3.4 Surface engineering approach. It has been realized that the physical and chemical properties of HCs can be optimized *via* surface engineering approaches, subsequently leading to a promoted electrochemical performance. Specially, the *in situ* method is an impressive one and has been carried out to achieve surface modification successfully. The *in situ* electropolymerization process was adopted by Wu *et al.*[135] to modify the surface of HC with 2,2-dimethylvinyl boric acid (DEBA), in which the C=C bonds formed a polymer network during the electrochemical test process. Accordingly, it resulted in the inhibition of the irreversible decomposition of the electrolyte and generation of a thinner SEI owing to the passive protecting layer. Therefore, an obviously improved ICE and cycle performance were acquired for HC-DEBA.

The desolvation process has been clarified to be one of the key reason that severely affects the Na^+ diffusion kinetics and the formation of an SEI. Recently, Zhou and coworkers proposed a step-by-step desolvation strategy to enable the rate capability and cycle stability of Na^+ storage in ester- and ether-based electrolytes.[136] A 3 Å zeolite molecular sieve film with a well-defined nanopore (3.2 Å) was selected to regulate the

desolvation process and the associated interfacial behavior. Then the desolvation process and charge transport dynamics of the molecular sieve film-coated HC were analyzed in detail, as shown in Fig. 11a and b, respectively. Specifically, the solvated Na^+ was not completely desolvated through the nanopore of the molecular sieve film and formed naked Na^+, but generated a solvent structure with higher aggregation, which can be regarded as partial desolvation or pre-desolvation and well demonstrated *via* Raman and IR spectroscopy on the zeolite molecular sieve film (Fig. 11c). Thus, the unique pre-desolvation process will lead to different interfacial charge transport kinetics. Therefore, the synergistic improvement in the Na^+ transport dynamics is beneficial for acquiring a fabulous rate capability, high specific capacity and cycle stability (Fig. 11d–f). This can be ascribed to the fact that the desolvation activation energy of the HC anode using the pre-desolvated electrolyte (10.87 kJ mol^{-1}) was significantly lower than that using the original 1 M $NaPF_6$-G2 electrolyte (21.87 kJ mol^{-1}) and promoted the formation of a thinner and inorganic-based SEI (3.1 nm), which greatly reduced the activation energy of Na^+ transport through the SEI (Fig. 11g and h). This special route
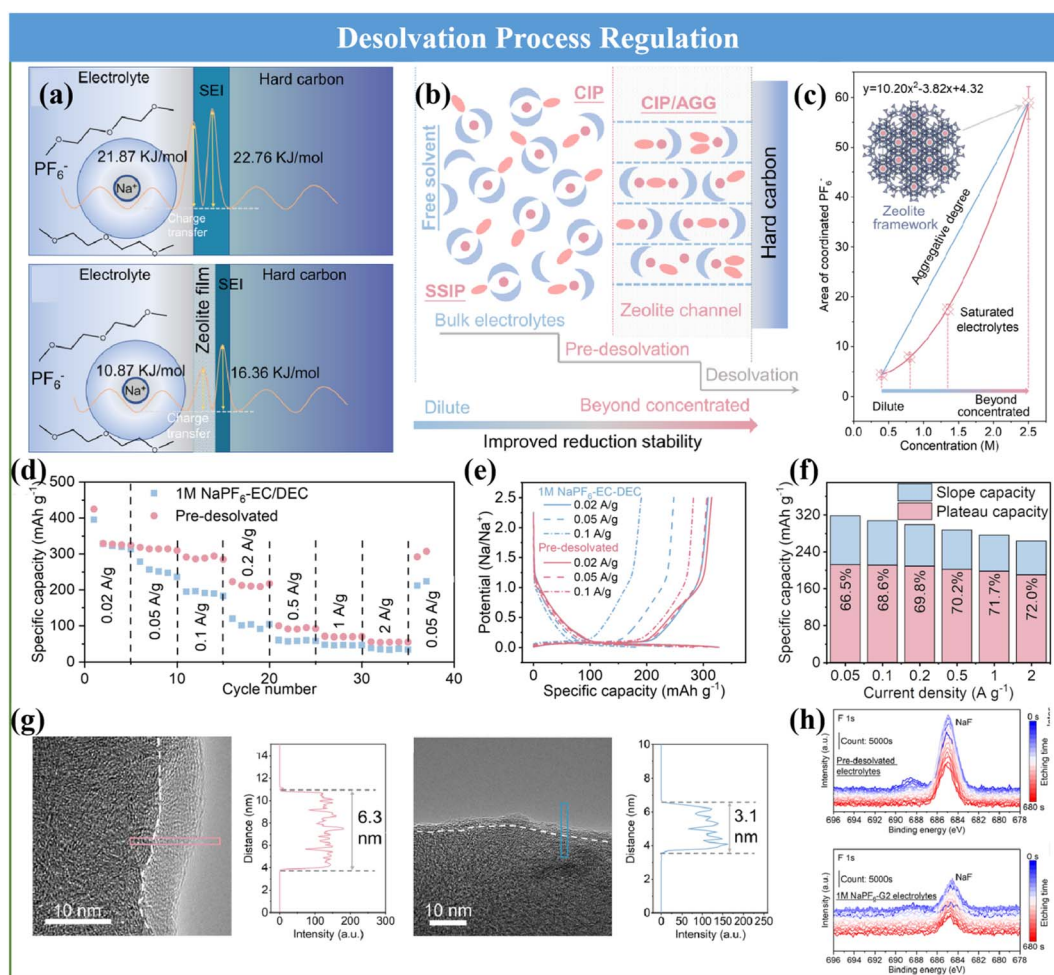

Fig. 11 (a) Comparison of the kinetics of desolvation and Na^+ transport through the SEI in different electrolytes. (b) Diagram of the step-by-step desolvation procedure. (c) Relationship between electrolyte concentration and coordinated PF_6^-. (d–f) Electrochemical performance of HC in different electrolytes. (g) TEM image of HC after 100 cycles in different electrolytes and the related SEI thickness profile. (h) NaF signal changes of SEI formed in different electrolytes at various etching times.
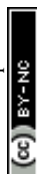
can provide novel possibilities for elevating the rate performance and cycle behavior of HC anode in SIBs.

Construction of a homogenous and inorganic-rich SEI on the HC anode plays a significantly important role in the electrochemical behaviors of SIBs. However, the constitution and thickness of the formed SEI layer originating from the employed ester electrolytes cannot satisfy the aforementioned needs. Motivated by this, recently, Bai and coworkers innovatively proposed a interfacial catalysis mechanism to gain the desirable SEI in the adopted ester electrolytes by accurately implanting C=O for reconstructing the surface functionality of HCs (Fig. 12a), which could be detected and observed by TEM (Fig. 12b) and XPS measurements.[137] Accordingly, the interfacial properties of the HC anode surface were optimized, and its Na storage performance was comprehensively improved (Fig. 12c and d). For the first time, an SEI layer with uniform and stable inorganic substances derived from the ester electrolyte was realized, and the structure–activity relationship between the

optimization of the interfacial property and the improvement in Na storage performance was further clarified (Fig. 12e and f). Besides, the interfacial catalysis mechanism of the C=O group inducing the formation of inorganic substances by the SEI was revealed, as seen in Fig. 12g. As a result, it effectively restrained the excessive solvent decomposition, and also obviously promoted the structural stability and interfacial Na$^+$ transfer of SEI on HCs. An fabulous advanced ICE of about 93.2%, ultra-high reversible capacity of about 379.6 mA h g^{-1} and superior cycling behavior (no obvious degradation in capacity over 10 000 cycles) could be achieved.

Overall, in the case of the post-processing step, whether it is structural modification or modulation of the interface between the electrode and electrolyte, it needs to be simple and easy with scaling-up potential to achieve effectively enhanced material properties without generating defects. Besides, it is necessary to ensure the homogeneity of the final products through these modification approaches when scaled up for practical production.
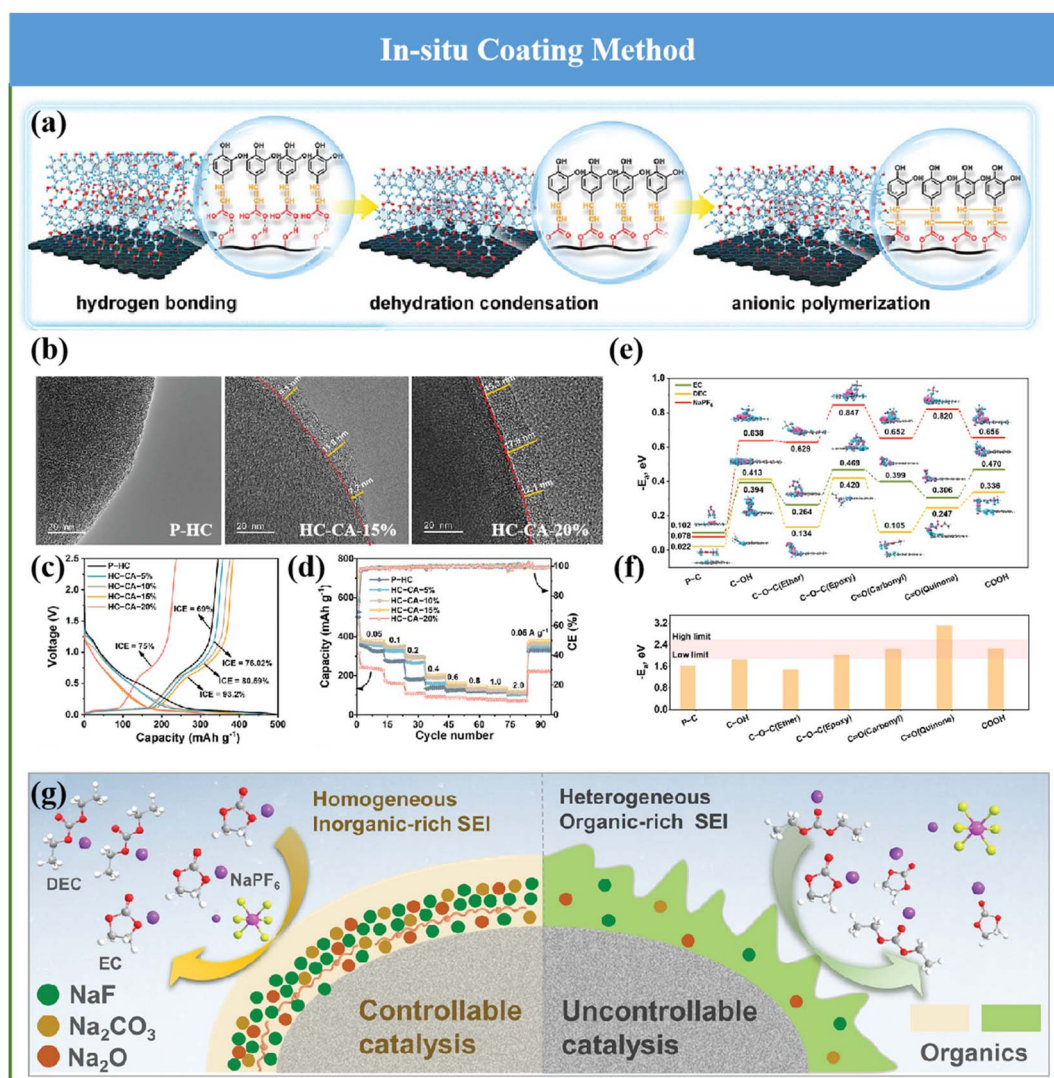

Fig. 12 (a) Illustration of the surface-functionality-reconstruction strategy of HC anodes, (b) TEM images of the HC anodes with different contents of CA, (c) GCD curves and (d) rate performances for HC anodes. (e) Binding energies of EC, DEC and NaPF$_6$ and (f) Na$^+$ adsorption energies by different oxygen-functional groups. (g) Diagram of SEI formation under a controllable catalysis mechanism in an ester electrolyte.
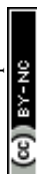
5. Theoretical calculations

Despite the enormous experiments undertaken towards the optimal process conditions to achieve high-performance HC anodes for SIBs, some experimental limitations still exist, such as difficulty in real-time observation and limited observational scales. In this regard, theoretical calculation approaches can be employed to solve the aforementioned challenges for the application of HC.

5.1 Annealing-molecular dynamics (MD) simulation

MD simulation refers to the method of combining theoretical and computational techniques to simulate or emulate the microscopic behavior of molecular motion, which can accurately describe various physical phenomena of deformation and evolution features for materials on the nanoscale, and further to extract the physical and mechanical parameters of nanomaterials. This advanced technology can not only get the trajectory of atoms, but also can observe various microscopic details in the process of atomic motion.

MD simulations are often used to generate realistic carbon models at tens of nanometers and predict their microstructure–property relationships, as presented in Fig. 13a.[138] Combining annealing-MD simulations and the Arrhenius framework, a series of large-scale molecular models for a cellulose-based HC anode was constructed to reproduce the main experimental characteristics at different annealing temperatures in Zhang's work.[139] Accordingly, the representative structural features and the detailed transformation information of each annealing stage at the atomic scale could be obtained. More interestingly, based on the resultant models, ReaxFF-MD could be applied to examine the sodium behavior in HCs with varying nanostructures. In the actual production process of HCs, it is difficult to use *in situ* tools to

observe the changes in their microstructures, and therefore simulation through theory becomes an effective means. By employing this method, Titirici and coworkers elucidated the mechanism of the remarkably accelerated pyrolysis from the quickly increased carbon sp² content under the multifield effect for the ultrafast synthesis of HCs *via* the SPS approach.[123] This meaningful method can give profitable guidance for atomic insight into the material design and sodium storage behavior of HCs for SIB.

5.2 Density functional theory (DFT)

DFT is a method to investigate the electronic structure of multi-electronic systems and often combined with related experiments as a complement and extension of the experimental disciplines. By studying the structure of materials (*e.g.*, bond lengths and vibrations), the mechanisms behind the matter can be further explored, which is widely used in the field of energy storage.

It can effectively predict the electronic structure of a material (such as its highest occupied molecular orbitals, lowest unoccupied electron energy level orbitals, Fermi energy level, and band gap). Meanwhile, the nature of electron transport, especially the transportation and diffusion of sodium ions can be predicted, thus achieving sodium conductivity. Furthermore, the prediction of the stability of battery systems can also be obtained based on the existing materials database. Particularly, the effect of different functional groups of HCs on sodium storage behaviors and different defects and layer spacing distances can also be calculated. Meanwhile, to support some experimental results, DFT can be applied to evaluate the binding energies and the density of states for anode materials (as shown in Fig. 13b) and even the electrode/electrolyte interface, providing new opportunities and insights to explore and understand the underlying Na⁺ storage mechanisms.[140,141]
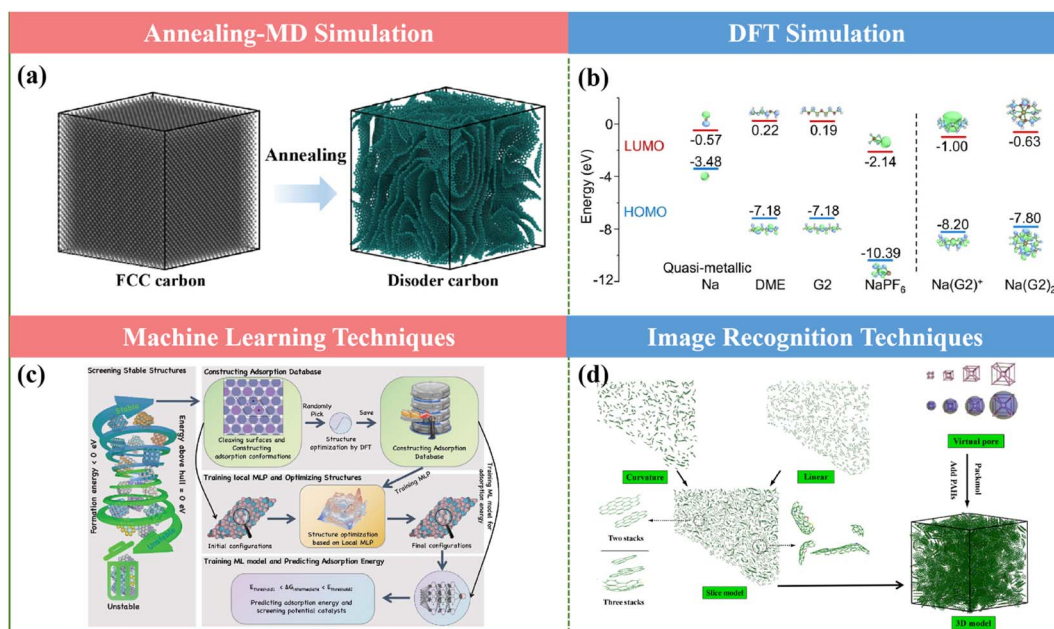

Fig. 13 Theoretical calculations: (a) annealing–MD simulation, (b) DFT simulation, (c) machine learning technique and (d) image recognition techniques.

5.3 Machine learning

At present, the design and development of materials mainly rely on the traditional "trial and error" experimental methods to prepare and test samples, which are associated with the drawbacks including long period, low efficiency, high cost and certain degree of inconsistency. Alternatively, the application of machine learning in the design and development of materials, the implied relationship between parameters can be extracted from a large number of experimental data (including composition, macroscopic properties, organizational structure, energy characteristics of the parameters and process parameters), and the property influencing factors and changing rules can be found, and the prediction model can be created to guide the design of new materials.

Machine learning is an efficient, accurate and scalable research tool and methodology that has emerged in recent years, which can be applied for electrochemical data analysis, prediction, and optimization (Fig. 13c). Particularly, machine learning techniques can bring more possibilities in the design of electrode materials for energy storage devices with the characteristics of high computational efficiency and accuracy.[142,143] Furthermore, they can not only predict the cost and properties of the materials, but also provide the prediction of the lifetime for the prepared materials. Therefore, they are encouraging methods established for screening electrode materials and can be extended to screening the synthesis methods for the preparation of HCs.

5.4 Image analysis technique

The typical material image characterization process including material preparation, structural characterization, and later image analysis and annotation all need to be tedious manually completed, not only showing low efficiency and high margin of error, but also will miss the differences of many tiny topological structures. This makes it difficult to fully understand the structural properties of the material, greatly reducing the possibility to discover new materials and new structures for application.

Regarding the development of HC applications, it is limited by the comprehension of their complicated microstructures. Alternatively, the distribution of structural features can contribute to the atomistic representations of HC, presenting some performance optimization approaches.[144] Particularly, it is worth noting that some parameters obtained from physical measurements, especially HRTEM, can be easily acquired by utilizing image analysis software (Fig. 13d).[145] Combined with XPS, SAXS, FT-IR, XRD, LDIMS, *etc.*, the molecular structure of HCs for SIBs can be investigated in great detail by creating a three-dimensional model and the structural ordering, pore size distribution, orientation, and chemical diversity can be successfully captured, which is expected to help the further exploration of the relationship between microstructure and electrochemical behavior.

Overall, the remarkable achievements from advanced theoretical calculation approaches are continuously developing to allow new discoveries and a better fundamental understanding of the structure/material evolution and energy storage mechanisms, and thus it is highly desirable to achieve high-performance HCs and realize their large-scale production.

6. Summary and outlook

With the increasing impact of lithium resource constraints, the development of SIBs has received significant attention and been boosted in recently. However, the progress of the anode side becomes the rate-determining step in this process. HCs are regarded as the most promising anode materials for commercialization in SIBs owing to their merits including low cost, abundant resources and high reversible specific capacity. Hence, rational design and effective strategies to regulate the structure of HC play an essential role in promoting the development of SIBs. The synthesis of HCs through various methods in the recent literature was summarized, and also the possibilities of their large-scale practical applications from potential laboratory technologies analyzed in this review. Specifically, the advanced strategies can be divided into two aspects, *i.e.*, those exhibiting great potential for scaled-up production and about frontier techniques (Fig. 14). Notably, the common characteristics of the methods with large-scale application prospects demonstrate low difficulty in scaling up production, high preparation efficiency, and overall enhancement in electrochemical performance for HC anode materials. Alternatively, the frontier techniques, for example, SC with tightened pore entrances *via* CVD coating, can inevitably suppress the formation of excessive SEI film and result in an obvious enhancement in ICE. Nevertheless, it is difficult to realize homogeneous coating *via* this unique method in large-scale production procedures. In addition, unprecedented rate capability and low-temperature electrochemical performance have been delivered for HCs through the ZnO-assisted bulk etching method. However, the tedious preparation steps and drop-wise process for polymerization reaction are major obstacles preventing its commercialization progress. Besides, the low-temperature oxygen plasma technique with non-destructive features for tailoring the surface chemistry of HCs has been successfully achieved. However, the precise regulation of the contents and configurations for different functional groups are still huge challenges.

Despite the encouraging achievements obtained to date, the development of SIBs is still in the early stages and the exploration of novel approaches to achieve high-performance HCs for large-scale production are still urgently needed. As mentioned, limitations still exist in the preparation efficiency and Na storage performance of HCs prepared by the traditional methods. The novel and advanced strategies, combined with the advantages of the advanced pre-treatment methods, advanced high-temperature carbonization approaches and advanced post-treating strategies, which realize large-scale production, while maintaining an excellent performance will show practical significance (Fig. 14a–l). In detail, in the traditional methods, their slow heating rate leads to long reaction times and lower yield, causing the high cost of final HC product, and the electrochemical performance of these HC product is also normal. In the case of the combination of the aforementioned advanced methods (Fig. 14c–i), on the one hand, the cost will increase due to the greater number of synthesis steps. On the other hand, the shorter reaction time will reduce the influence of the increased cost, and the electrochemical
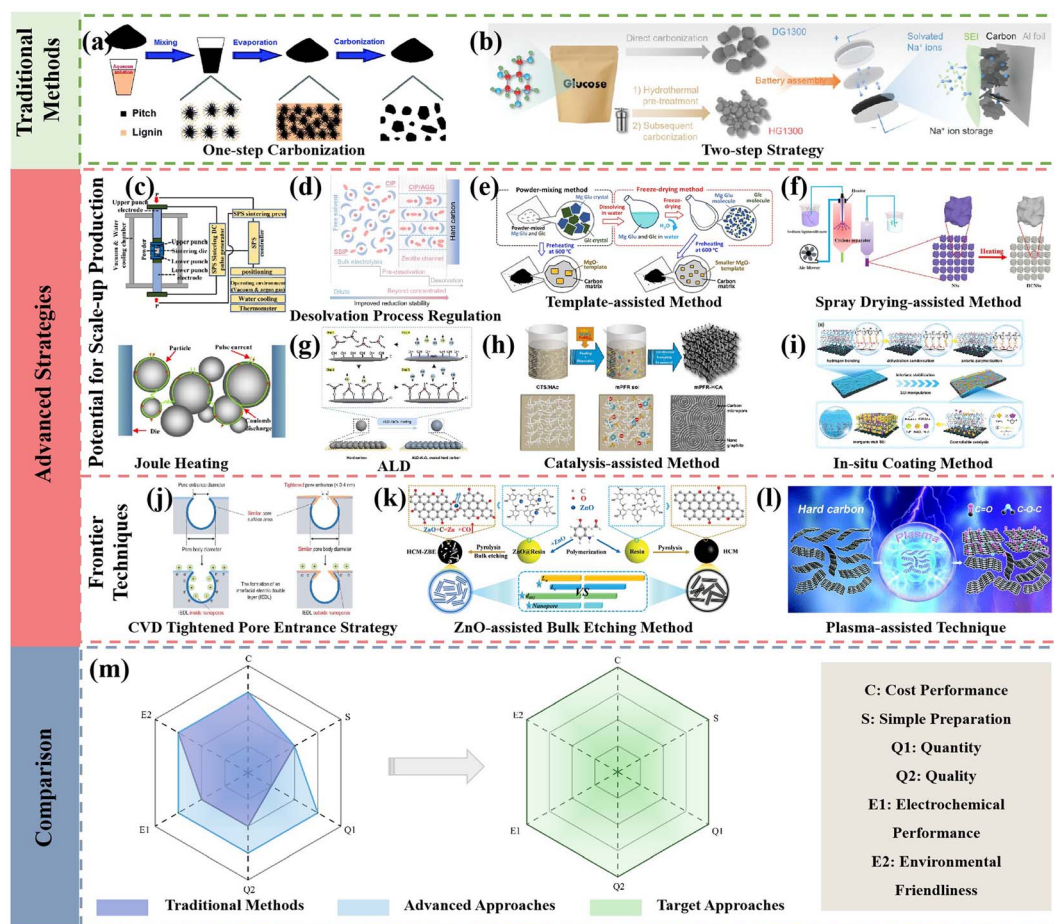
Fig. 14 Illustration of traditional methods and advanced strategies and comparison between traditional, advanced methods and target approaches in the future for HC preparation.

performance (including rate capability, ICE, and capacity) will achieve huge promotion by modifying the preparation method (Fig. 14m). Overall, there are still lots of challenges remaining to realize the target. Specifically, the follow-up investigation can be conducted from the following aspects:

(1) Common precursors for the preparation of HCs include biomass, synthetic polymers and fossil fuels. Significant performances differs a lot according to various precursors. Meanwhile, because of the different sources of precursor feedstocks, there are also noteworthy differences in the cost and composition of HCs. Consequently, the selection of precursors and accumulation of process technology are the key factors in the development of HCs.

(2) Seek new synthesis methods and technologies to optimize the synthesis process and develop new instruments and equipment with the merits of scalable, efficient, and rapid features for the preparation of HCs to realize high efficiency and high performance. Besides, the establishment of mature testing and evaluation systems should be created to provide more information to guide the design of materials.

(3) Combining the advantages of different advanced methods including template-assisted strategies, Joule heating, plasma, and ALD to achieve an overall improvement in the electrochemical behaviors of HCs. In addition, the optimization

of other components of the battery system is also of significant importance for the performance of HC anodes, and more research is required for their refinement.

(4) Accurately and controllably constructing advanced methods to clarify the conformational relationship of method–structure–performance for HCs and related exploration for their scaled-up production. Furthermore, it is urgently needed to extend the means of measurement and characterization and strengthen the research on the sodium storage mechanism for the professional customization of HC anodes.

(5) To achieve a systematic meaningful result, advanced theoretical calculation methods with experimental processes can be combined to reduce the trial and error time, improve the production efficiency and save costs, further resulting in novel ground-breaking discoveries and providing valuable guidance for the scaled-up production of HCs.

(6) Developing research collaborations between commercial product users and HCs manufacturers and strengthening communication of desired characteristics and final goals of products can help to regulate the microstructures, resulting in the higher-quality implementation of HCs. Simultaneously, considerations from cross-industry or academic-industrial collaborations can also foster the development of HCs.

Overall, thus far, although the exploration of new approaches to realize high-performance HCs is limited and there are still some challenges existing, the acceleration of research and development of related technologies is highly encouraged to overcome the unsolved issues. Furthermore, the comparison and combination of traditional and advanced methods is expected to achieve more perfect preparation approaches in the future (as shown in Fig. 14m). We hope that the comprehensive description in this review can provide beneficial guidance to actualize the truly rational design of advanced HC anodes aimed at the industrialization of SIBs and assist in formulating design rules for developing high-end advanced electrode materials for energy storage devices.

Author contributions

C. W. wrote the manuscript. X. W. and S. C. structured this review. Y. Y., Y. Z., H. X., and X. H. collected papers related to the topic. The manuscript was revised by all authors.

Conflicts of interest

There are no conflicts to declare.

Acknowledgements

References

1 J. Hwang, S. Myung and Y. Sun, *Chem. Soc. Rev.*, 2017, **46**, 3529–3614.

2 Z. Ni, C. Bao, Y. Liu, W. Wu, S. Chen, X. Dai, B. Chen, B. Hartweg, Z. Yu, Z. Holman and J. Huang, *Science*, 2020, **367**, 1352–1358.

3 K. Jiao, J. Xuan, Q. Du, Z. Bao, B. Xie, B. Wang, Y. Zhao, L. Fan, H. Wang, Z. Hou, S. Huo, N. P. Rrandon, Y. Yin and M. D. Guiver, *Nature*, 2021, **595**, 361–369.

4 C. Zhao, Q. Wang, Z. Yao, J. Wang, B. Sánchez-Lengeling, F. Ding, X. Qi, Y. Lu, X. Bai, B. Li, H. Li, A. Aspuru-Guzik, X. Huang, C. Delmas, M. Wagemaker, L. Chen and Y. S. Hu, *Science*, 2020, **370**, 708.

5 B. Li, B. Xi, Z. Feng, Y. Lin, J. Liu, J. Feng, Y. Qian and S. Xiong, *Adv. Mater.*, 2018, **30**, 1705788.

6 B. Yin, S. Liang, D. Yu, B. Cheng, I. L. Egun, J. Lin, X. Xie, H. Shao, H. He and A. Pan, *Adv. Mater.*, 2021, **33**, 2100808.

7 H. Xia, X. Zhu, J. Liu, Q. Liu, S. Lan, Q. Zhang, X. Liu, J. K. Seo, T. Chen, L. Gu and Y. S. Meng, *Nat. Commun.*, 2018, **9**, 5100.

8 Y. Ye, Y. Zhao, T. Zhao, S. Xu, Z. Xu, J. Qian, L. Wang, Y. Xing, L. Wei, Y. Li, J. Wang, L. Li, F. Wu and R. Chen, *Adv. Mater.*, 2021, **33**, 2105029.

9 C. Zhao, Z. Yang, X. Zhou, Z. Hao, J. Chen, Z. Wang, X. Chen, X. Wu, L. Li, L. Li, L. Jiao and S. Chou, *Adv. Funct. Mater.*, 2023, 2303457.

10 N. Lege, X. He, Y. Wang, Y. Lei, Y. Yang, J. Xu, M. Liu, X. Wu, W. Lai and S. Chou, *Energy Environ. Sci.*, 2023, **16**, 5688–5720.

11 H. Hou, X. Qiu, W. Wei, Y. Zhang and X. Ji, *Adv. Energy Mater.*, 2017, **7**, 1602898.

12 J. Peng, W. Zhang, Q. Liu, J. Wang, S. Chou, H. Liu and S. Dou, *Adv. Mater.*, 2022, **34**, 2108384.

13 J. Yan, H. Li, K. Wang, Q. Jin, C. Lai, R. Wang, S. Cao, J. Han, Z. Zhang, J. Su and K. Jiang, *Adv. Energy Mater.*, 2021, **11**, 2003911.

14 Z. Tang, R. Zhang, H. Wang, S. Zhou, Z. Pan, Y. Huang, D. Sun, Y. Tang, X. Ji, K. Amine and M. Shao, *Nat. Commun.*, 2023, **14**, 6024.

15 H. Wang, P. Feng, F. Fu, X. Yu, D. Yang, W. Zhang, L. Niu and X. Qiu, *Carbon Neutralization*, 2022, **1**, 277–297.

16 P. Senguttuvan, G. Rousse, V. Seznec, J. Tarascon and M. Palacin, *Chem. Mater.*, 2011, **23**, 4109–4111.

17 A. Rudola, K. Saravanan, C. Mason and P. Balaya, *J. Mater. Chem. A*, 2013, **1**, 2653–2662.

18 H. Kim, J. Kwon, B. Lee, J. Hong, M. Lee, S. Park and K. Kang, *Chem. Mater.*, 2015, **27**, 7258–7264.

19 W. Luo, M. Allen, V. Raju and X. Ji, *Adv. Energy Mater.*, 2014, **4**, 1400554.

20 L. Zhang, W. Wang, S. Lu and Y. Xiang, *Adv. Energy Mater.*, 2021, **11**, 2003640.

21 B. Cao, H. Liu, B. Xu, Y. Lei, X. Chen and H. Song, *J. Mater. Chem. A*, 2016, **4**, 6472.

22 Y. Sun, S. Guo and H. Zhou, *Adv. Energy Mater.*, 2019, **9**, 1800212.

23 Q. Wang, C. Zhao, Y. Lu, Y. Li, Y. Zheng, Y. Qi, X. Rong, L. Jiang, X. Qi, Y. Shao, D. Pan, B. Li, Y. Hu and L. Chen, *Small*, 2017, **13**, 1701835.

24 Y. Yang, C. Wu, X. He, J. Zhao, Z. Yang, L. Li, X. Wu, L. Li and S. Chou, *Adv. Funct. Mater.*, 2023, **34**, 2302277.

25 Q. Meng, B. Chen, W. Jian, X. Zhang, S. Sun, T. Wang and W. Zhang, *J. Power Sources*, 2023, **581**, 233475.

26 M. Pelaez-Samaniego, S. Mood, J. Garcia-Nunez, T. Garcia-Perez, V. Yadama and M. Garcia-Perez, *Sustainable Biochar for Water and Wastewater Treatment*, 2022, vol. 39.

27 D. Stevens and J. Dahn, *J. Electrochem. Soc.*, 2000, **147**, 1271.

28 Y. Lu, C. Zhao, X. Qi, Y. Qi, H. Li, X. Huang, L. Chen and Y. Hu, *Adv. Energy Mater.*, 2018, **8**, 1800108.

29 R. Xu, Z. Yi, M. Song, J. Chen, X. Wei, F. Su, L. Dai, G. Sun, F. Yang, L. Xie and C. Chen, *Carbon*, 2023, **206**, 94–104.

30 B. Xiao, T. Rojo and X. Li, *ChemSusChem*, 2019, **12**, 133–144.

31 X. Dou, I. Hasa, D. Saurel, C. Vaalma, L. Wu, D. Buchholz, D. Bresser, S. Komaba and S. Passerini, *Mater. Today*, 2019, **23**, 87–104.

32 Y. Ding and Z. Qiao, *Adv. Mater.*, 2022, **34**, 2206025.

33 Y. Cao, L. Xiao, M. Sushko, W. Wang, B. Schwenzer, J. Xiao, Z. Nie, L. Saraf, Z. Yang and J. Liu, *Nano Lett.*, 2012, **12**, 3783–3787.

34 C. Bommier, T. Surta, M. Dolgos and X. Ji, *Nano Lett.*, 2015, **15**, 5888–5892.

35 Y. Li, Y. Hu, M. Titirici, L. Chen and X. Huang, *Adv. Energy Mater.*, 2016, **6**, 1600659.

36 Y. Morikawa, S. Nishimura, R. Hashimoto, M. Ohnuma and A. Yamada, *Adv. Energy Mater.*, 2020, **10**, 1903176.

37 N. Sun, Z. Guan, Y. Liu, Y. Cao, Q. Zhu, H. Liu, Z. Wang, P. Zhang and B. Xu, *Adv. Energy Mater.*, 2019, **9**, 1901351.

38 X. He, J. Zhao, W. Lai, R. Li, Z. Yang, C. Xu, Y. Dai, Y. Gao, X. Liu, L. Li, G. Xu, Y. Qiao, S. Chou and M. Wu, *ACS Appl. Mater. Interfaces*, 2021, **13**, 44358–44368.

39 X. Chen, J. Tian, P. Li, Y. Fang, Y. Fang, X. Liang, J. Feng, J. Dong, X. Ai, H. Yang and Y. Cao, *Adv. Energy Mater.*, 2022, **12**, 2200886.

40 L. Lai, J. Li, Y. Deng, Z. Yu, L. Wei and Y. Chen, *Small Struct.*, 2022, **3**, 2200112.

41 D. Chen, W. Zhang, K. Luo, Y. Song, Y. Zhong, Y. Liu, G. Wang, B. Zhong, Z. Wu and X. Guo, *Energy Environ. Sci.*, 2021, **14**, 2244–2262.

42 Y. Li, L. Mu, Y. Hu, H. Li, L. Chen and X. Huang, *Energy Storage Mater.*, 2016, **2**, 139.

43 H. Wang, Z. Shi, J. Jin, C. Chong and C. Wang, *J. Electroanal. Chem.*, 2015, **755**, 87.

44 J. Jin, Z. Shi and C. Wang, *Electrochim. Acta*, 2014, **141**, 302–310.

45 L. Xiao, Y. Cao, W. Henderson, M. Sushko, Y. Shao, J. Xiao, W. Wang, M. Engelhard, Z. Nie and J. Liu, *Nano Energy*, 2016, **19**, 279–288.

46 Q. Li, Y. Zhu, P. Zhao, C. Yuan, M. Chen and C. Wang, *Carbon*, 2018, **129**, 85–94.

47 Y. Li, Y. Hu, H. Li, L. Chen and X. Huang, *J. Mater. Chem. A*, 2016, **4**, 96–104.

48 P. Wang, X. Zhu, Q. Wang, X. Xu, X. Zhou and J. Bao, *J. Mater. Chem. A*, 2017, **5**, 5761.

49 X. Dou, I. Hasa, M. Hekmatfar, T. Diemant, R. Behm, D. Buchholz and S. Passerini, *ChemSusChem*, 2017, **10**, 2668–2676.

50 S. Alvin, D. Yoon, C. Chandra, R. Susanti, W. Chang, C. Ryu and J. Kim, *J. Power Sources*, 2019, **430**, 157.

51 M. Dahbi, M. Kiso, K. Kubota, T. Horiba, T. Chafik, K. Hida, T. Matsuyama and S. Komaba, *J. Mater. Chem. A*, 2017, **5**, 9917–9928.

52 C. Wang, J. Huang, H. Qi, L. Cao, Z. Xu, Y. Cheng, X. Zhao and J. Li, *J. Power Sources*, 2017, **358**, 85–92.

53 D. Qin, F. Zhang, S. Dong, Y. Zhao, G. Xu and X. Zhang, *RSC Adv.*, 2016, **6**, 106218.

54 V. Simone, A. Boulineau, A. Geyer, D. Rouchon, L. Simonin and S. Martinet, *J. Energy Chem.*, 2016, **25**, 761–768.

55 Y. Zhu, M. Chen, Q. Li, C. Yuan and C. Wang, *Carbon*, 2018, **129**, 695–701.

56 S. Huang, Z. Li, B. Wang, J. Zhang, Z. Peng, R. Qi, J. Wang and Y. Zhao, *Adv. Funct. Mater.*, 2018, **28**, 1706294.

57 N. Zhang, Q. Liu, W. Chen, M. Wan, X. Li, L. Wang, L. Xue and W. Zhang, *J. Power Sources*, 2018, **378**, 331–337.

58 D. Yoon, J. Hwang, W. Chang and J. Kim, *ACS Appl. Mater. Interfaces*, 2018, **10**, 569–581.

59 Q. Zhang, X. Liu, L. Yan, Q. Ren, Z. Yang, S. Liu and Z. Shi, *Chem. Eng. J.*, 2022, **448**, 137628.

60 Z. Zhu, F. Liang, Z. Zhou, X. Zeng, D. Wang, P. Dong, J. Zhao, S. Sun, Y. Zhang and X. Li, *J. Mater. Chem. A*, 2018, **6**, 1513–1522.

61 M. Song, Z. Yi, R. Xu, J. Chen, J. Cheng, Z. Wang, Q. Liu, Q. Guo, L. Xie and C. Chen, *Energy Storage Mater.*, 2022, **51**, 620–629.

62 L. Yan, J. Wang, Q. Ren, L. Fan, B. Liu, L. Zhang, L. He, X. Mei and Z. Shi, *Chem. Eng. J.*, 2022, **432**, 133257.

63 Q. Jin, K. Wang, H. Li, W. Li, P. Feng, Z. Zhang, W. Wang, M. Zhou and K. Jiang, *Chem. Eng. J.*, 2021, **417**, 128104.

64 J. Wang, J. Zhao, X. He, Y. Qiao, L. Li and S. L. Chou, *Sustainable Mater. Technol.*, 2022, **33**, e00446.

65 Q. Li, X. Liu, Y. Tao, J. Huang, J. Zhang, C. Yang, Y. Zhang, S. Zhang, Y. Jia, Q. Lin, Y. Xiang, J. Cheng, W. Lv, F. Kang, Y. Yang and Q.-H. Yang, *Natl. Sci. Rev.*, 2022, **9**, nwac084.

66 X. Wu, S. Wu, C. Wu, X. Zhang, Z. Jiang, S. Liu and N. Li, *Carbon*, 2022, **191**, 112–121.

67 A. Kamiyama, K. Kubota, D. Igarashi, Y. Youn, Y. Tateyama, H. Ando, K. Gotoh and S. Komaba, *Angew. Chem., Int. Ed.*, 2021, **60**, 5114–5120.

68 M. Yuan, C. Meng, A. Li, B. Cao, Y. Dong, D. Wang, X. Liu, X. Chen and H. Song, *Small*, 2022, **18**, 2105738.

69 K. Kubota, S. Shimadzu, N. Yabuuchi, S. Tominaka, S. Shiraishi, M. Abreu-Sepulveda, A. Manivannan, K. Gotoh, M. Fukunishi, M. Dahbi and S. Komaba, *Chem. Mater.*, 2020, **32**, 2961–2977.

70 F. Zhang, Y. Yao, J. Wan, D. Henderson, X. Zhang and L. Hu, *ACS Appl. Mater. Interfaces*, 2017, **9**, 391–397.

71 J. Zhao, X. X. He, W. H. Lai, Z. Yang, X. H. Liu, L. Li, Y. Qiao, Y. Xiao, L. Li, X. Wu and S. L. Chou, *Adv. Energy Mater.*, 2023, **13**, 2300444.

72 X. X. He, W. H. Lai, Y. Liang, J. H. Zhao, Z. Yang, J. Peng, X. H. Liu, Y. X. Wang, Y. Qiao, L. Li, X. Wu and S. L. Chou, *Adv. Mater.*, 2023, 2302613.

73 P. Bai, Y. He, X. Zou, X. Zhao, P. Xiong and Y. Xu, *Adv. Energy Mater.*, 2018, **8**, 1703217.

74 H. Au, H. Alptekin, A. C. S. Jensen, E. Olsson, C. A. O'Keefe, T. Smith, M. Crespo-Ribadeneyra, T. F. Headen, C. P. Grey, Q. Cai, A. J. Drew and M. M. Titirici, *Energy Environ. Sci.*, 2020, **13**, 3469–3479.

75 B. Zhang, C. M. Ghimbeu, C. Laberty, C. Vix-Guterl and J. M. Tarascon, *Adv. Energy Mater.*, 2016, **6**, 1501588.

76 A. Gomez-Martin, J. Martinez-Fernandez, M. Ruttert, M. Winter, T. Placke and J. Ramirez-Rico, *Chem. Mater.*, 2019, **31**, 7288–7299.

77 Z. Guo, Z. Xu, F. Xie, J. Jiang, K. Zheng, S. Alabidun, M. CrespoŔRibadeneyra, Y. Hu, H. Au and M. Titirici, *Adv. Mater.*, 2023, 2304091.

78 Z. Huang, X. Qiu, C. Wang, W. Jian, L. Zhong, J. Zhu, X. Zu and W. Zhang, *J. Energy Storage*, 2023, **72**, 108406.

79 R. Chen, X. Li, C. Cai, H. Fan, Y. Deng, H. Yu, L. Mai and L. Zhou, *Small*, 2023, 2303790.

80 L. Shi, Y. Sun, W. Liu, F. Zhao, G. Cheng, F. Zeng and J. Ding, *Electrochim. Acta*, 2023, **459**, 142557.

81 H. Tonnoir, D. Huo, C. Davoisne, A. Celzard, V. Fierro, D. Saurel, M. E. Marssi, M. Benyoussef, P. Meunier and R. Janot, *Carbon*, 2023, **208**, 216–226.

82 C. Fan, R. Zhang, X. Luo, Z. Hu, W. Zhou, W. Zhang, J. Liu and J. Liu, *Carbon*, 2023, **205**, 353–364.

83 T. Xu, X. Qiu, X. Zhang and Y. Xia, *Chem. Eng. J.*, 2023, **452**, 139514.

84 C. Cai, Y. Chen, P. Hu, T. Zhu, X. Li, Q. Yu, L. Zhou, X. Yang and L. Mai, *Small*, 2022, **18**, 2105303.

85 J. Han, I. Johnson, Z. Lu, A. Kudo and M. Chen, *Nano Lett.*, 2021, **21**, 6504–6510.

86 H. Zhang, H. Ming, W. Zhang, G. Cao and Y. Yang, *ACS Appl. Mater. Interfaces*, 2017, **9**, 23766–23774.

87 Y. Liu, H. Dai, Y. An, L. Fu, Q. An and Y. Wu, *J. Mater. Chem. A*, 2020, **8**, 14993.

88 Y. Zheng, Y. Lu, X. Qi, Y. Wang, L. Mu, Y. Li, Q. Ma, J. Li and Y. S. Hu, *Energy Storage Mater.*, 2019, **18**, 269–279.

89 K. Hong, L. Qie, R. Zeng, Z. Yi, W. Zhang, D. Wang, W. Yin, C. Wu, Q. Fan, W. Zhang and Y. Huang, *J. Mater. Chem. A*, 2014, **2**, 12733.

90 X. Dou, I. Hasa, D. Saurel, M. Jauregui, D. Buchholz, T. Rojo and S. Passerini, *ChemSusChem*, 2018, **11**, 3276–3285.

91 C. Matei Ghimbeu, B. Zhang, A. M. Yuso, B. Réty and J. M. Tarascon, *Carbon*, 2019, **153**, 634–647.

92 X. Huang, H. Yu, J. Chen, Z. Lu, R. Yazami and H. H. Hng, *Adv. Mater.*, 2014, **26**, 1296–1303.

93 X. Dou, C. Geng, D. Buchholz and S. Passerini, *APL Mater.*, 2018, **6**, 047501.

94 A. Adamson, R. Väli, M. Paalo, J. Aruväli, M. Koppel, R. Palm, E. Härk, J. Nerut, T. Romann, E. Lust and A. Jänes, *RSC Adv.*, 2020, **10**, 20145–20154.

95 Y. Li, Y. Lu, Q. Meng, A. C. S. Jensen, Q. Zhang, Q. Zhang, Y. Tong, Y. Qi, L. Gu, M. M. Titirici and Y. S. Hu, *Adv. Energy Mater.*, 2019, **9**, 1902852.

96 R. Väli, A. Jänes, T. Thomberg and E. Lust, *J. Electrochem. Soc.*, 2016, **163**, A1619.

97 Z. Xu, J. Wang, Z. Guo, F. Xie, H. Liu, H. Yadegari, M. Tebyetekerwa, M. P. Ryan, Y. S. Hu and M. M. Titirici, *Adv. Energy Mater.*, 2022, **12**, 2200208.

98 L. Xiao, H. Lu, Y. Fang, M. L. Sushko, Y. Cao, X. Ai, H. Yang and J. Liu, *Adv. Energy Mater.*, 2018, **8**, 1703238.

99 J. A. Gerbec, D. Magana, A. Washington and G. F. Strouse, *J. Am. Chem. Soc.*, 2005, **127**, 15791–15800.

100 A. V. Murugan, T. Muraliganth and A. Manthiram, *J. Phys. Chem. C*, 2008, **112**, 14665–14671.

101 Y. Zhu, S. Murali, M. D. Stoller, A. Velamakanni, R. D. Piner and R. S. Ruoff, *Carbon*, 2010, **48**, 2118–2122.

102 T. Chen, L. Pan, T. Lu, C. Fu, D. Chua and Z. Sun, *J. Mater. Chem. A*, 2014, **2**, 1263–1267.

103 Nagmani and S. Puravankara, *ACS Appl. Energy Mater.*, 2020, **3**, 10045–10052.

104 N. Cuesta, I. Cameán, A. Arenillas and A. B. García, *Microporous Mesoporous Mater.*, 2020, **308**, 110542.

105 B. H. Hou, Y. Y. Wang, Q. L. Ning, W. H. Li, X. T. Xi, X. Yang, H. J. Liang, X. Feng and X. L. Wu, *Adv. Mater.*, 2019, **31**, 1903125.

106 D. Zhao, Q. Ru, S. Hu and X. Hou, *Ionics*, 2017, **23**, 897–905.

107 K. Wang, F. Sun, H. Wang, D. Wu, Y. Chao, J. Gao and G. Zhao, *Adv. Funct. Mater.*, 2022, **32**, 2203725.

108 X. Zhao, Y. Ding, Q. Xu, X. Yu, Y. Liu and H. Shen, *Adv. Energy Mater.*, 2019, **9**, 1803648.

109 X. Li, J. Sun, W. Zhao, Y. Lai, X. Yu and Y. Liu, *Adv. Funct. Mater.*, 2022, **32**, 2106980.

110 H. Zhang, W. Zhang and F. Huang, *Chem. Eng. J.*, 2022, **434**, 134503.

111 M. Guo, H. Zhang, Z. Huang, W. Li, D. Zhang, C. Gao, F. Gao, P. He, J. Wang, W. Chen, X. Chen, M. Terrones and Y. Wang, *Small*, 2023, 2302583.

112 Z. L. Yu, S. Xin, Y. You, L. Yu, Y. Lin, D. W. Xu, C. Qiao, Z. H. Huang, N. Yang, S. H. Yu and J. B. Goodenough, *J. Am. Chem. Soc.*, 2016, **138**, 14915–14922.

113 W. Zhong, D. Cheng, M. Zhang, H. Zuo, L. Miao, Z. Li, G. Qiu, A. Cheng and H. Zhang, *Carbon*, 2022, **198**, 278–288.

114 Q. Jin, K. Wang, W. Li, H. Li, P. Feng, Z. Zhang, W. Wang, M. Zhou and K. Jiang, *J. Mater. Chem. A*, 2020, **8**, 22613–22619.

115 Z. Qiao, S. Hwang, X. Li, C. Wang, W. Samarakoon, S. Karakalos, D. Li, M. Chen, Y. He, M. Wang, Z. Liu, G. Wang, H. Zhou, Z. Feng, D. Su, J. S. Spendelow and G. Wu, *Energy Environ. Sci.*, 2019, **12**, 2830–2841.

116 I. Elizabeth, B. P. Singh, S. Trikha and S. Gopukumar, *J. Power Sources*, 2016, **329**, 412–421.

117 X. Yin, Z. Lu, J. Wang, X. Feng, S. Roy, X. Liu, Y. Yang, Y. Zhao and J. Zhang, *Adv. Mater.*, 2022, **34**, 2109282.

118 Z. Lu, J. Wang, W. Feng, X. Yin, X. Feng, S. Zhao, C. Li, R. Wang, Q. A. Huang and Y. Zhao, *Adv. Mater.*, 2023, **35**, 2211461.

119 K. M. Wyss, D. X. Luong and J. M. Tour, *Adv. Mater.*, 2022, **34**, 2106970.

120 L. Lai, J. Li, Y. Deng, Z. Yu, L. Wei and Y. Chen, *Small Struct.*, 2022, **3**, 2200112.

121 Y. Yao, Z. Huang, P. Xie, S. D. Lacey, R. J. Jacob, H. Xie, F. Chen, A. Nie, T. Pu, M. Rehwoldt, D. Yu, M. R. Zachariah, C. Wang, R. Shahbazian-Yassar, J. Li and L. Hu, *Science*, 2018, **359**, 1489–1494.

122 F. Jiang, Y. Yao, B. Natarajan, C. Yang, T. Gao, H. Xie, Y. Wang, L. Xu, Y. Chen, J. Gilman, L. Cui and L. Hu, *Carbon*, 2019, **144**, 241–248.

123 Y. Zhen, Y. Chen, F. Li, Z. Guo, Z. Hong and M. M. Titirici, *Proc. Natl. Acad. Sci. U. S. A.*, 2021, **118**, e2111119118.

124 P. Zhang, Y. Shu, Y. Wang, J. Ye and L. Yang, *J. Mater. Chem. A*, 2023, **11**, 2920–2932.

125 M. Song, Q. Song, T. Zhang, X. Huo, Z. Lin, Z. Hu, L. Dong, T. Jin, C. Shen and K. Xie, *Nano Res.*, 2023, **16**, 9299–9309.

126 X. Chen, N. Sawut, K. Chen, H. Li, J. Zhang, Z. Wang, M. Yang, G. Tang, X. Ai, H. X. Yang, Y. Fang and Y. Cao, *Energy Environ. Sci.*, 2023, **16**, 4041–4053.

127 C. Shen, C. Wang, T. Jin, X. Zhang, L. Jiao and K. Xie, *Nanoscale*, 2022, **14**, 8959–8966.

128 X. Tang, F. Xie, Y. Lu, Z. Chen, X. Li, H. Li, X. Huang, L. Chen, Y. Pan and Y. S. Hu, *Nano Res.*, 2023, **16**, 12579–12586.

129 S. J. An, J. Li, C. Daniel, D. Mohanty, S. Nagpure and D. L. Wood, *Carbon*, 2016, **105**, 52–76.

130 Y. Zhao, L. V. Goncharova, A. Lushington, Q. Sun, H. Yadegari, B. Wang, W. Xiao, R. Li and X. Sun, *Adv. Mater.*, 2017, **29**, 1606663.

131 H. Lu, X. Chen, Y. Jia, H. Chen, Y. Wang, X. Ai, H. Yang and Y. Cao, *Nano Energy*, 2019, **64**, 103903.

132 C. Yu, Y. Li, H. Ren, J. Qian, S. Wang, X. Feng, M. Liu, Y. Bai and C. Wu, *Carbon Energy*, 2023, **5**, e220.

133 W. Li, J. Yang, Z. Wu, J. Wang, B. Li, S. Feng, Y. Deng, F. Zhang and D. Zhao, *J. Am. Chem. Soc.*, 2012, **134**, 11864–11867.

134 F. L. Yang, W. Zhang, Z. X. Chi, F. Q. Cheng, J. T. Chen, A. M. Cao and L. J. Wan, *Chem. Commun.*, 2015, **51**, 2943–2945.

135 C. X. Yu, Y. Li, Z. H. Wang, X. R. Wang, Y. Bai and C. Wu, *Rare Met.*, 2022, **41**, 1616–1625.

136 Z. Lu, C. Geng, H. Yang, P. He, S. Wu, Q. H. Yang and H. Zhou, *Proc. Natl. Acad. Sci. U. S. A.*, 2022, **119**, e2210203119.

137 M. Liu, F. Wu, Y. Gong, Y. Li, Y. Li, X. Feng, Q. Li, C. Wu and Y. Bai, *Adv. Mater.*, 2023, **35**, 2300002.

138 Y. Wang, Y. Zhu and H. Wu, *Phys. Chem. Chem. Phys.*, 2021, **23**, 10290–10302.

139 J. Li, C. Peng, J. Wang, J. Li and H. Zhang, *Diamond Relat. Mater.*, 2022, **129**, 109355.

140 H. Fang, S. Gao, M. Ren, Y. Huang, F. Cheng, J. Chen and F. Li, *Angew. Chem., Int. Ed.*, 2023, **62**, e202214717.

141 Y. Li, Y. Yuan, Y. Bai, Y. Liu, Z. Wang, L. Li, F. Wu, K. Amine, C. Wu and J. Lu, *Adv. Energy Mater.*, 2018, **8**, 1702781.

142 L. Chen, Y. Tian, X. Hu, S. Yao, Z. Lu, S. Chen, X. Zhang and Z. Zhou, *Adv. Funct. Mater.*, 2022, **32**, 2208418.

143 W. Wu and Q. Sun, *ACS Mater. Lett.*, 2022, **4**, 175–180.

144 P. Pré, G. Huchet, D. Jeulin, J.-N. Rouzaud, M. Sennour and A. Thorel, *Carbon*, 2013, **52**, 239–258.

145 J. Li, T. Li, C. Peng, J. Li and H. Zhang, *J. Electrochem. Soc.*, 2022, **169**, 070517.